The LUVOIR Extreme Coronagraph for Living Planetary Systems (ECLIPS) I: searching and characterizing exoplanetary gems

L. Pueyo[a], C. Stark [a], R. Juanola-Parramon [b], N. Zimmerman [b], M. Bolcar [b], A. Roberge [b], G. Arney [b], G. Ruane [c], A.J. Riggs [c], R. Belikov [d], D. Sirbu [d] D. Redding [c], R. Soummer[a], I. Laginja [a], S. Will [e]

[a] Space telescope Science Institute, 3700 San Martin Drive, Baltimore, MD 21218, USA
[b] NASA Goddard Space Flight Center, 8800 Greenbelt Rd., Greenbelt, MD, 20771 USA
[c] Jet Propulsion Laboratory, California Institute of Technology, 4800 Oak Grove Dr., Pasadena, CA 91109, USA
[d] Nasa AMES, Moffett Blvd, Mountain View, CA 94035, USA
[e] The Institute of Optics, University of Rochester, 275 Hutchison Road Rochester, NY 14627, USA

ABSTRACT

Detection and characterization of Earth-like planets around nearby stars using the direct imaging technique is a key scientific objective of future NASA astrophysics flagship missions. As a result, dedicated exoplanet instruments are being studied for the Large UV/Optical/Infrared Surveyor (LUVOIR) and the Habitable Exoplanet Imager (HabEx) mission concepts. In this paper we discuss the Extreme Coronagraph for Living Planetary Systems (ECLIPS) instrument of LUVOIR. ECLIPS will be capable of providing starlight suppression levels of ten orders of magnitude over a broad range of wavelengths in order to detect and characterize the light reflected from potentially Earth-like planets. It will also allow future astronomers to study in great detail the diversity of exoplanets.

First, we review the main science drivers and emphasize those that are the most stressing on the instrument design. We then present the overall parameters of the instrument (general architecture and back-end camera). We delve into the details of the static coronagraph masks, which have a significant impact on the scientific productivity of the mission. We discuss the choices the LUVOIR team made in order to maximize the discovery yield of exoEarth candidates. We then present our work on the technological feasibility of such an instrument, focusing in particular on the image stability necessary to achieve ten orders of magnitude of starlight extinction over hours of exposure. We present our error budget and show that using a combination of instrument level (low and high order wavefront sensors) and observatory level telemetry can yield an overall architecture that meets these requirements. Finally, we discuss future technology development efforts that will mature these technologies.

Keywords: planetary systems - techniques: coronagraphy, wavefront control

1. INTRODUCTION

1.1 Scientific Context

Decades of exoplanet observations using a variety of techniques have revealed a nearly fantastical universe, filled with exoplanets of an astounding variety. While some of these planetary systems may resemble our own, others are anything but: evaporated cores of gas giants, gaseous "sub-Neptune" planets, and giant planets on retrograde, eccentric orbits. The outcome of planetary formation and system evolution may indeed be as chaotic as the equations of motion that control them. But we have yet to answer, do other Earth-like planets exist? And do they provide an opportunity for life to arise elsewhere? Answering these questions, by searching for and

Further author information: (Send correspondence to Laurent Pueyo)
Laurent Pueyo: E-mail: pueyo@stsci.edu

Techniques and Instrumentation for Detection of Exoplanets IX, edited by Stuart B. Shaklan, Proc. of SPIE
Vol. 11117, 1111703 · © 2019 SPIE · CCC code: 0277-786X/19/$21 · doi: 10.1117/12.2530722

characterizing other potentially Earth-like worlds around Sun-like stars, is within our grasp for the first time. Indeed, conducting this ambitious experiment is one of the key recommendations of the recent NAS Exoplanet Science Strategy Report,[1] and a core focus for two of the four large mission concept studies commissioned by NASA in preparation for Astro2020.[2,3]

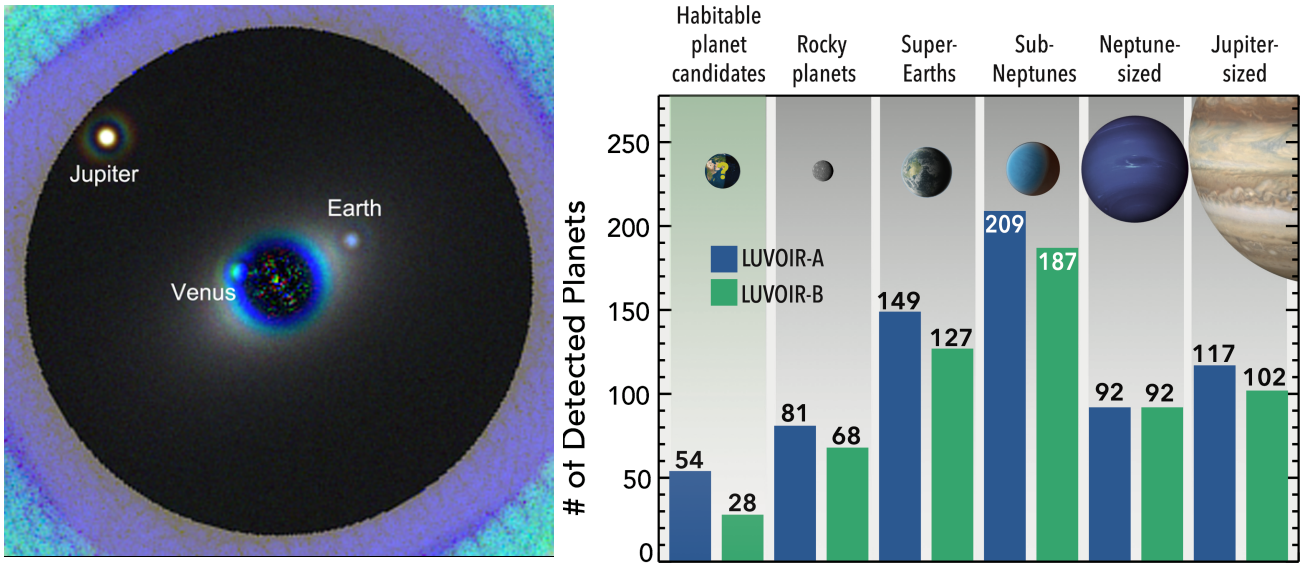

Figure 1: Left: *Simulated image of an exosolar system with a coronagraph of a large segmented telesecope.*[4] *Credit: L. Pueyo, M. N'Diaye (STScI)/A. Roberge (NASA GSFC).* Right: *Exoplanet discovery yields*[5] *based on a two year census of Earth-like exoplanets with LUVOIR A and LUVOIR B. Credit: C. Stark (STScI)/J. Friedlander (NASA GSFC).*

The LUVOIR science goals are very ambitious, with observing capabilities articulated around the following key science themes:

The census of Earth-like exoplanets: Reveal the character of rocky exoplanets and measure the fraction that are truly Earth-like. This requires determining the thermal/chemical states of rocky planet atmospheres by measuring the abundances of key molecular species, including water vapor and other greenhouse gases. This also requires measuring orbits (and ideally masses) of as many of these planets as possible. These measurements involve multiple visits to each star and pushed the LUVOIR team towards coronagraph architectures.

The search for life: Search for the byproducts of life in seemingly Earth-like planets. This requires similar observing tools used for the exoEarth census to probe the atmospheres of those planets for biosignature gases and find the first signs of life outside our home planet. By targeting exoplanets with sizes and orbits similar to Earth's and host stars similar to the Sun, we hope to increase our chances of finding, and *recognizing*, extraterrestrial life.

The solar system's place in the universe: Exoplanet discoveries over the past couple of decades show that the planet formation process is robust and leads to a wide range of outcomes, most of them very different from our solar system. By exploring the character of many kinds of exoplanets, including types that do not exist in the solar system, like warm Jupiters, sub-Neptunes, and super-Earths, LUVOIR will reveal what is typical about our own system and what is unusual.

Together these science goals require detecting and characterizing some of the faintest objects ever imaged in sample sizes that can allow for meaningful statistical queries. This in turn requires a) a large collecting area, one that is commensurate with other ambitious astrophysical observations (not discussed here, see LUVOIR interim report[3]), and b) an exquisitely designed and stable coronagraphic instrument. Over the past few years the LUVOIR team has studied two large observatory concepts: LUVOIR A, a 15-m on-axis segmented aperture, and LUVOIR B, an 8-m off-axis segmented aperture. Mirror segmentation is required to achieve the desired

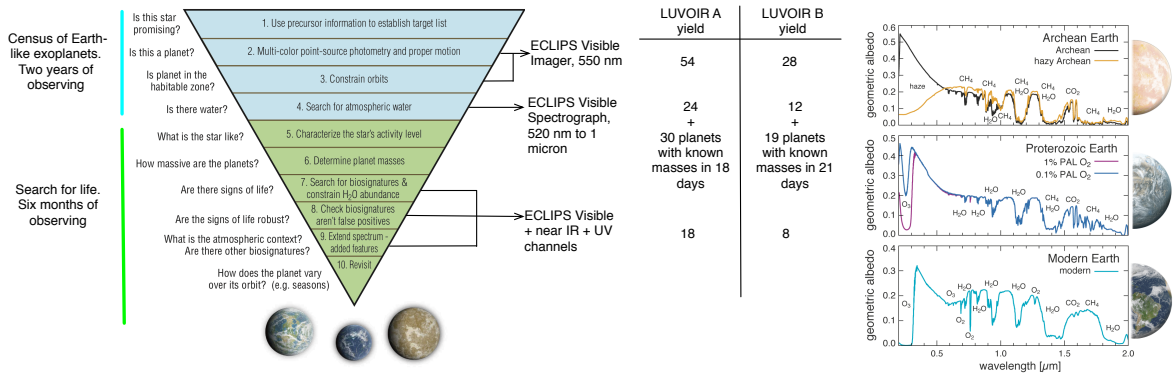

Figure 2: Left: Sequence of LUVOIR ECLIPS observations associated with the census of Earth-like exoplanets and search for life science cases. Middle: Spectroscopic yields for the three science cases of ECLIPS (characterization of planets with known masses is used as a proxy for the "exoplanet diversity" case. Credit: T. B. Griswold (NASA GSFC). Right: Predicted evolution of the earth reflected spectrum across cosmic ages. This highlights the important of spectroscopy over a wide range of UVOIR wavelengths in order to obtain key observables to understand the emergence of life on potentially habitable planets. Credit: G. Arney (NASA GSFC).

collecting area given the mass and volume constraints set by the launch vehicle. Both LUVOIR A and B include a coronagraph instrument, the Extreme Coronagraph for Living Planetary Systems (ECLIPS), that would serve as the workhorse for these investigations. This paper describes in detail the design trades associated with this instrument concept and the differences in implementation for the LUVOIR A and B concepts.

1.2 Technological Context

Direct imaging observations of exoplanets are extremely challenging. From a radiometry standpoint, exoEarths are as faint as any extragalactic source observed to date, and photon-starved spectroscopy is required to measure molecular content and potentially detect biosignatures. Moreover, exoplanets are hiding in the glare of their host stars, which are roughly ten billion times brighter than the light reflected by an Earth-twin's atmosphere. Precisely optimized coronagraphs are needed to block stellar photons, while at the same time preserving as much light as possible from the planet. Finally, this level of stellar rejection has to be maintained during the long exposures associated with exoplanet spectroscopy. This requires an observatory, including spacecraft, telescope, and instrument, whose imaging properties are exquisitely stable over a broad range of temporal and spatial scales.

These three top level considerations (sensitivity, starlight suppression, and image stability) translate into very stringent performance requirements for all subsystems in the science production chain. In this paper we describe the building blocks underlying the ECLIPS instrument concept, alongside the various trades the LUVOIR team considered before converging on this design. Throughout this document, we highlight key enabling technologies that have been rapidly matured over the past decade. The field of exoplanet imaging is young, but is rapidly devising and demonstrating innovative technologies. The ECLIPS concept draws from these past two decades of innovation, and represents the most scientifically compelling version of an exoplanet imaging instrument for LUVOIR that could be built using today's state-of-the-art for all subsystems. Future work will further mature these technologies and firmly establish that their integration within a large astrophysics mission enables the ambitious science motivating LUVOIR.

2. BACK END INSTRUMENT

2.1 Science driver: exoplanet characterization

Spectroscopic reconnaissance of a large sample of exoEarth candidates is a cornerstone science case for LUVOIR. Such observations account for two and a half years of the LUVOIR DRM. The left panel of Fig. 2 illustrates how spectroscopic observations of earth-analogs at various ages can test ongoing hypotheses regarding the emergence

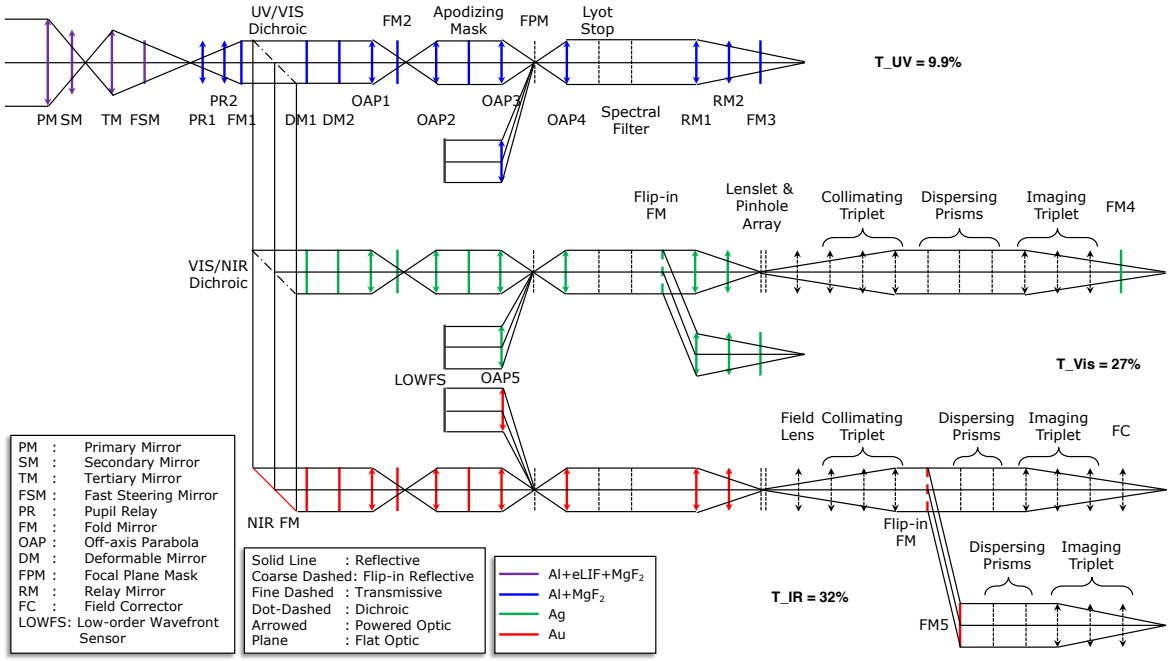

Figure 3: Schematic of the ECLIPS optical train. The overall architecture, splitting the beam in three channels with dichroics, is driven by the three different detector technologies needed in UV, visible and near IR. The throughput in each channel is driven by the large number of optics required to place DMs and coronagraph masks in multiple conjugate planes of the telescope pupil. This general architecture has been adopted for the ECLIPS instruments on both LUVOIR concepts A and B. Credit: M. Bolcar (GSFC)

of life. In this first section we discuss the trades associated with the design of the back-end imagers and spectrographs. These drive wavelength coverage, spectral resolution and signal-to-noise ratio (SNR).

Quantitive retrieval of a wide range of molecular atmospheric abundances will require broad spectral coverage. The benefits of broad wavelength coverage have been demonstrated for hot Jupiters[6] and cloudy browns dwarfs;[7] simulations show that it will also be the case for the small rocky planets that LUVOIR will observe.[8] At shorter wavelengths, the observable bandpass is limited by the reflectivity of the optics in the UV, as well as increasingly stringent surface roughness requirements. This bounds the shortest wavelength of ECLIPS at $\sim$ 250 nm. The long wavelength cutoff is set by the steep onset of the warm observatory's thermal background at 1.8 μm. To date there is no single detector technology that covers this entire spectral range; the beam coming from the telescope is thus split at the entrance of ECLIPS into separate UV, optical, and near-IR channels. Each channel has its own set of optics, as shown on Fig 3, optimized for its wavelength range. Because of a coronagraph's need to have multiple pupil images for masks and deformable mirrors, the total number of reflections is much larger in a coronagraphic instrument such as ECLIPS than a direct imager such as LUVOIR's High Definition Imager (HDI). As a result, the overall throughput of each channel is driven by the number of reflections in the optical train and the reflectivities of the optics.

2.2 Technology, state of the art

There are two key technologies driving the backend instrument: astronomical detectors and spectrograph architectures. Detection of bio-signatures requires high SNR spectra of point sources of magnitude 27 and fainter. Thus read noise, as well as other sources of detector noise, must be minimized. The beginning-of-life noise parameters for the WFIRST Coronagraph Instrument's (CGI) EMCCD are close to those needed for LUVOIR's visible wavelength detector. Any future advancement in low noise/high density detector technologies, applicable

to a wide range of astrophysical observations, would enhance the ECLIPS performance beyond what is presented here.

Over the past decade, tremendous strides have been made using ground-based Integral Field Spectrographs (IFS) for the atmospheric characterization of gas giant exoplanets. The ECLIPS IFS capitalizes on this recent progress. More recently, point spectrographs have also been used for direct exoplanet spectral characterization. Combining this alternative technique with fiber injection could have tremendous advantages for ECLIPS. While we did not select a fiber-injected spectrograph for ECLIPS, this trade should be revisited when ECLIPS reaches phase A.

2.3 Imaging and detectors

2.3.1 Overall architecture:

Each channel features a post-coronagraph imager with a filter wheel. Because the spectral bandwidth of Wavefront Sensing and Control (WFSC) is assumed to be smaller than the bandwidth of each channel,[9] each channel is split into a series of sequential bandpasses, whose edges overlap for photometric calibration purposes. In principle the WFSC bandpass could be larger than the numbers adopted for LUVOIR A and B (20%). However, we conservatively chose values on par with what WFIRST-CGI will demonstrate (18% bandpass baselined in Phase A).[10] In spite of the large number of filters, the mass and volume associated with wheels is well within the margins allocated to the ECLIPS instruments on both the LUVOIR A and B concepts. However, sequential observation with different filters is one of the main drivers of longer spectroscopic observing times described on Fig. 2; future WFSC algorithms that broaden bandpass, potentially at the expense of contrast or field of view, may significantly decrease the time required to obtain spectra covering a broad range of wavelengths. The field of view for LUVOIR A is split among different coronagraphs that provide a set of Inner Working Angles (IWA) and Outer Working Angles (OWA) that enable exploration of stars at distances from a few parsecs to 50 parsecs. This is a result of the coronagraph mask technology chosen for LUVOIR A (see below). Just like filters these masks can be chosen sequentially.

Detector technologies:

Visible: the baseline technology for the visible (515–1030 nm) channel is an e2v EMCCD, with a format of 1024×1024, 13 μm pixels for the imager and 4096×4096 for the IFS . This technology is based on a silicon CCD with low-noise, on-chip, multiplication gain register (1000×). It is the baseline detector for the WFIRST CGI. We assumed zero read noise (in photon-counting mode), a median dark current of 3×10^{-5} e-/pix/sec (a factor of ∼3 better than that measured by the WFIRST CGI project[11,12]), and a clock induced charge of 1×10^{-3} e-/pix/frame (a factor of ∼20 improvement compared to the WFIRST CGI) for our radiometry calculations. We assume a high QE (90%) out to 1000 nm for efficient detection of atmospheric water vapor (though we note that if this cannot be obtained, a slightly more challenging water vapor feature near 800 nm will suffice with only small impacts to the exoplanet science yield).

Near-IR: the baseline technology for the near-IR is a Teledyne HAWAII 4RG with SIDECAR ASIC, with a format of 4096×4096, 13 μm pixels. This technology HgCdTe detectors, indium bump-bonded to a CMOS circuit, with SIDECAR ASIC Focal Plane Electronics. It is the baseline detector for the WFIRST wide-field instrument as well as JWST-NIRCam. We assumed a median read noise < 10 e-/pix at 100 kHz and 77 K, and a Median Dark Current: 2×10^{-3} e-/pix/sec (measured 90–110 K) for our radiometry calculations.

UV : the baseline technology is similar to the Visible channel except that the detector surface has been δ-doped processed. We assumed the same characteristic as the visible channel detector, however this technology is not fully mature and requires development.

The field of view and sampling of each imaging channel are summarized in Fig. 4. The imaging field of view goes well beyond the outer edge of the habitable zone of nearby stars, in order to accommodate observing programs covering the full range of exoplanet types, including outer giant planets.

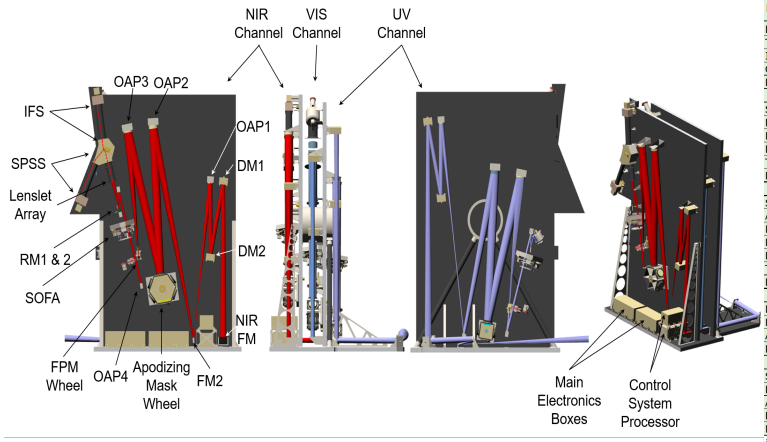

Parameter	Units	Value		
		UV	VIS	NIR
Raw Contrast	-		$1x10^{-10}$	
Total Bandpass	nm	200 - 525	515 - 1030	1000 - 2000
Inner Working Angle	-	4 λ/D	3.5 λ/D	3.5 λ/D
Outer Working Angle	-	40 λ/D	64 λ/D	64 λ/D
RMS Wavefront Error	nm	14	37	71
Spectrometer Lenslet Array Parameters				
Sampling at Lenslet Array	-	-	Nyquist at 515 nm	Nyquist at 1000 nm
Lenslet Diameter	μm	-	124	120
Pinhole Diameter	μm	-	30	40
Lenslet Packing	-	-	Square	Hexagonal
Total Lenslet Count	-	-	72,300	128,000
F/# at Lenslet Array	-	-	481.5	248.0
Integral Field Spectrometer Detector Parameters				
Sampling at Detector	-	-	Nyquist at 515 nm	Nyquist at 1000 nm
Average Optical Throughput	%		23.8	32.5
Pixel Size	μm	-	12	10
Magnification	-	-	1 : 1.47	1 : 1
F/# at Detector	-	-	11.8	\
Total Spectral Length*	pixels	-	34	20
Resovling Power		-	140	70
Single Point Source Spectrometer				
Pixel Size	μm	-	-	10
F/# at Detector	-	-	-	8.0
Average Optical Throughput	%	-	-	32.6
Resovling Power	-	-	-	200.0
Imaging Camera Parameters				
Sampling at Detector	-	Nyquist at 200 nm	Nyquist at 515 nm	-
F/# at Detector	-	130.0	50.5	-
Average Optical Throughput	%	9.9	27.7	-
Effective Focal Length	mm	2,628	1,020	-
Pixel Size	μm	13	13	-

*Includes isolation pixels.

Figure 4: Left*: Opto-mechanical packaging of the ECLIPS -A instrument.* Right*: Properties of the ECLIPS-A imagers and spectrographs. The opto-mechanical packaging, imaging field of view, and sampling are different for ECLIPS on LUVOIR-B, but follow the same guiding principles as for LUVOIR A. Credit: M. Bolcar (GSFC)*

2.4 Spectrographs

The imager is the only science detector in the UV channel. The visible and near-IR channels feature both an imager and a spectrograph. For spectroscopy, we considered both IFS[13] and fiber-fed spectrograph (FFS) architectures.[14] The pros and cons of each solution are listed below:

- **IFS pros**: This technology has a long heritage of exoplanet observations from the ground.[15–17] It is an intrinsically multiplexed design. That is: the spectrum of multiple planets (or background sources) can be obtained at the same time, which makes the observations more efficient. The continuum of each planet's spectrum, essential to measure absolute molecular abundances, is preserved. Furthermore, all coronagraphs operating in the exoEarth contrast regime must use dedicated wavefront sensing and control loops to null the residual starlight across the image search region. Again by virtue of the optically multiplexed spatial and spectral information, the IFS parallelizes this control loop in wavelength, reducing the operational overheads associated with each scientific observation.
- **IFS cons**: The majority of the detector real estate (where planets are absent) is not used. There is a constraining relationship between spectrograph field of view, resolution, and the number of pixels.[10] As a result a) resolutions of $\sim>100$, are difficult to achieve in the IFS configuration without sacrificing field of view, even with years of vigorous detector technology development. Therefore the detector-limited IFS field of view could preclude spectral characterization of outer giant planets for the nearest stars unless they happen to be in a gibbous phase during observation.
- **hi-res FFS pros:** Detector real estate does not limit spectral resolution. Both coherent starlight suppression (via fiber injection[14]) and post-processing gains using cross correlation with spectral templates[18,19] are possible with this architecture . This potentially relaxes the requirements on the wavefront control system. This technique will be tested in multiple ground based observatories over the next decade.[14,20,21] Ongoing technology work involves TRL 6 characterization of Fiber injection unit and the integration of a slit based point spectrograph for the WFIRST coronagraph.
- **hi-res FFS cons:** The cross correlation technique cannot measure absolute molecular abundances and achromatic fiber injection needs to be demonstrated in order to confidently measure the continuum of the planet's spectra. Because the spectrum of only one object at a time can be obtained, the observing efficiency of this design is inferior to the one of the IFS. Coupling the planet signal to the injection fiber on a remote space telescope might present operation difficulties that have not been explored as of today.

For the visible channel, the multiplex efficiency of the IFS considerably reduces observing time (as compared to FFS) during the candidate confirmation phase of the "The census of Earth-like exoplanets" DRM. Recent

developments in multiplexed fiber injection technologies might change this rationale over the next few years.[22] Since the IR channel will be dedicated to the characterization of detected planets, it is solely equipped with a IFS and point spectrographs (without fiber injection). The resolution of the latter was chosen based on a trade between the information content in the CO_2 absorption feature in the near-IR bandpass and the noise associated with the number of pixels over which the spectrum will be dispersed. The resolution currently baselined precludes the use of cross correlation techniques at higher resolution.[19] However should such methods mature over the next few years,[14] the baseline ECLIPS design can easily be revised to feature higher resolution.

3. CORONAGRAPH: THE STATIC PROBLEM

3.1 Architecture Science driver: exoEarth candidate yields

Here we addresses the design and manufacturing of the static starlight suppression system (assuming that the optics alignment does not change with time). The work presented here greatly benefited from three years of community activity under the umbrella of the NASA Exoplanet Exploration Program's Segmented Coronagraph Design Analysis (SCDA) program. This multi-institution effort has thoroughly explored the relationship between segmented aperture geometry and coronagraph performance. In this context, the main the performance metrics of a given coronagraph design for a given aperture are:

- Starlight suppression for perfectly aligned optics and assuming that the star is point source.
- Sensitivity of this starlight suppression to observed stellar angular size (large apertures yield resolved image of stars) along with sensitivity to generic misalignments.
- Off-axis point source (i.e., planet) throughput as a function of separation.
- Off-axis point source PSF sharpness
- Bandwidth of the coronagraph design (if less than WFSC bandwidth)

These metrics can then be used as input parameters for a Design Reference Mission (DRM). Such DRMs calculate an expected yield of discovered planets of a given type, which can be used to measure the scientific impact of a given coronagraph design. Sensitivity to generic misalignment is also used to estimate how difficult the wavefront stability problem will be to address (see discussions in the next section). Optimizing ECLIPS means securing the largest sample of detected exoplanets with a given telescope aperture. This sample ought to contain a sufficiently large pool of potentially Earth-like planets to be followed up with deep spectroscopy. While LUVOIR DRMs did include exoplanet populations over the broad range of properties (see Fig. 1), the the coronagraph masks were designed to maximize the total number of expected exoEarth candidates. The details of such yield calculations are given in Stark et al.[23] In this section, we first present the coronagraph designs studied by the LUVOIR team, from both design and technology readiness standpoints. We then discuss the solutions baselined for LUVOIR concepts A and B, underlying the yield numbers presented in Fig. 1, and the trades associated with our design choices. Along the way we also considered a number of telescope aperture geometries, though we do not discuss them in this paper and focus only on the two selected apertures for LUVOIR A and B.

3.2 Technology: state of the art

Up until five years ago, very few coronagraphs could work with on-axis and/or segmented apertures. Recent theoretical breakthroughs, along with the strong momentum spurred by the WFIRST CGI, have established that a wide array of solutions now exist for any observatory architecture. Moreover, WFIRST and other technology demonstration efforts are currently maturing the manufacturing technologies and operations procedures of critical components (masks and deformable mirrors). It is quite remarkable that, over the course of five years, the astronomical instrumentation community shifted away from questioning the fundamental feasibility of a coronagraph with LUVOIR to investigating how to maximize the planet's flux at the science detector, or how to minimize sensitivity to stellar angular size. This increase in the granularity/complexity of the questions asked by instrument designers stems from a) tremendous strides in the sophistication of the numerical techniques used for coronagraph optimization b) our ability to now use high fidelity simulated coronagraph images for yield calculations. The designs and yields presented in this paper are anchored in today's state of the art in coronagraphy. However, given the rapid progress that has occurred over the past two years, we expect that they will be

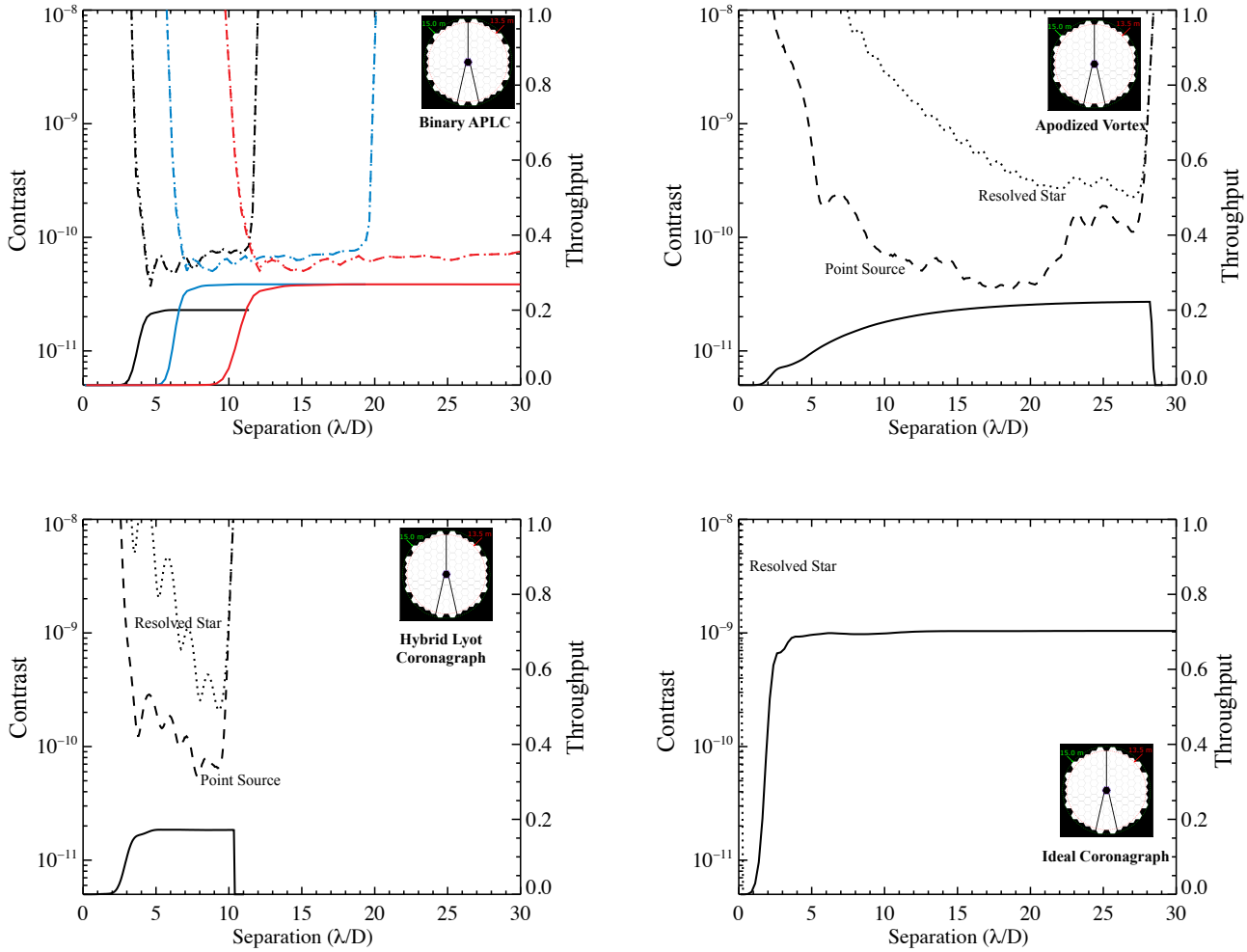

Figure 5: Coronagraph designs considered for LUVOIR A. Dashed and dotted lines indicate the contrast (left vertical axis) as a function of angular separation for point sources and resolved stars (0.1 λ/D), respectively. Solid lines indicate the planet throughput (right vertical axis), measured as the encircled energy in a 0.7 λ/D disk, as a function of angular separation. With a central obscuration only the binary APLC designs submitted by the community to the LUVOIR team achieve an efficient compromise between robustness to resolved stellar angular size and throughput to be used on a large number of stars. Note, however, that in theory ideal coronagraphs (lower right) can achieve high contrast and throughput regardless of stellar diameter, although it remains to be determined whether such solutions can be practically built. Credit: C. Stark (STScI), R. Soummer (STScI), N. Zimmermann (GSFC), K. Fogarty (Caltech), A.J. Riggs (JPL), R. Belikov (NASA Ames).

superseded in the near future; indeed, noticeable design improvements have occurred in just the last few months. This will further bolster the science productivity of LUVOIR when it flies.

3.3 Binary Apodized Pupil Lyot Coronagraph

3.3.1 Design

The design of binary APLCs is based on two decades of optimization of binary masks for space-based coronagraphs.[24] Because it is based on a numerical optimization over a given arbitrary entrance aperture, the binary APLC can accommodate any telescope geometry.[4,25] Intrinsically this architecture has modest throughput and

typically larger inner working angles (IWA), since it filters the light from the planet at the beginning of the optical train. This can be mitigated by optimizing the size of the focal plane mask, field stop, and Lyot stop in conjunction with the apodizer. Robustness to stellar angular size and generic misalignments can be included in the mask design by forcing the core of the occulted starlight diffraction pattern to be smaller than the focal plane mask.[26] These designs have a finite outer working angle (OWA) that is often much smaller than the limit set by the finite number of actuators on the DMs. As a result a combination of masks is necessary to map the habitable zone of the complete LUVOIR target list. Performances of these designs are given on Fig. 5.

3.3.2 Component level maturity

Binary apodizers for monolithic telescopes have been tested both in air[27,28] and in vacuum[29] for over a decade. Since this technology was selected for the WFIRST CGI it has been tested with an obscured aperture, in static[30] and dynamic environments,[31] and using an IFS as a back end instrument.[10] Steady progress toward contrasts around 10^{-9} in a relevant environment has been occurring under the context of WFIRST CGI. The WFIRST CGI masks are manufactured using a black silicon coating on a reflective surface[32] (in order to minimize the amount of transmissive optics). This technology will be at the TRL 9 for LUVOIR. Alternative manufacturing techniques using carbon nanotubes are also being tested in air.[33]

3.4 Vortex Coronagraph

3.4.1 Design

Historically the Vortex Coronagraph was developed as technique to perfectly cancel starlight for an unobscured circular aperture.[34] The presence of a circular central obscuration can be mitigated using apodizers,[35,36] at the expense of throughput. Segment gaps and secondary support structures can then be mitigated using DMs. Several algorithms have been presented over the years to do so.[37–41] The optical layout of the dual-DM subsystems needs to be optimized in order to maximize starlight suppression and minimize off-axis PSF distortion and jitter induced beam walk.[42] Overall Vortex designs have smaller IWA and higher throughput than APLC solutions, though the throughput grows slowly with separation. On a circular aperture they are naturally robust to stellar angular size at high (>4) topological charges (number of phase warps of the focal plane mask). However, this property is not true in the presence of a central obscuration. Apodizers can be tailor designed to recover this property, but at a prohibitively large reduction in throughput.[43] Performances of these designs are illustrated in Figs. 5 and 6.

3.4.2 Component level maturity

Vortex masks for visible wavelengths were first built and tested using liquid crystal technologies.[44,45] Intrinsic chromaticity due to mask transmission can be mitigated either using multiple layers or cross polarizers to filter out the leakage.[44,45] Vacuum tests have demonstrated 10^{-8} contrasts at small IWA, but have been limited by internal mask reflections and incoherent light.[46] Other technologies include annular grove masks, that have been successfully deployed on the ground-based telescopes at longer near-IR wavelengths. Should their maturity keep progressing, this technology will be an excellent option for the ECLIPS IR channel, for which stars are smaller in units of λ/D. Ongoing work is also focused on using the scalar vortex mask in order to alleviate the need for polarizers. This work is at an early stage.

3.5 Phase Induced Amplitude Apodization Coronagraph

3.5.1 Design

PIAA coronagraphs are based on two aspheric mirrors that remap the light in order to change the illumination over the projected telescope aperture while preserving photons.[47] These mirror pairs can be used with either an opaque focal plane mask (FPM) or with complex masks in order to improve the IWA. While initially conceived of for circular unobscured apertures, this family of coronagraphs can operate with any telescope geometry.[48] Early WFIRST studies showed that designs with complex masks featured a strong coupling between IWA and robustness to generic low order misalignments. This feature makes phase-masked PIAA designs great candidates for the ECLIPS IR channel (longer wavelengths require smaller IWA, but less robustness). For the visible channel, we considered designs with opaque FPMs.[49] Performances of these designs are given on 6 for LUVOIR B.

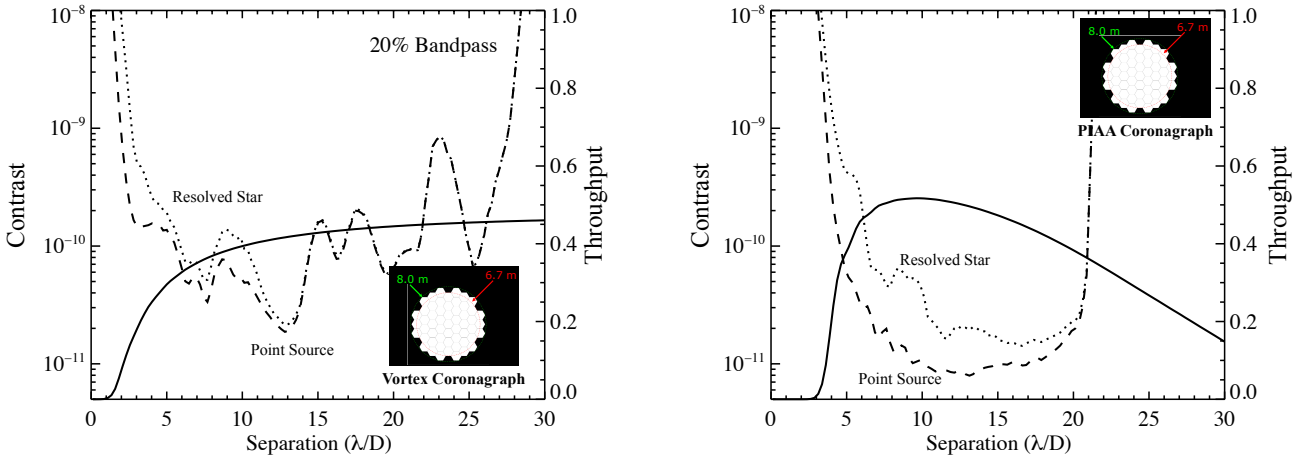

Figure 6: Coronagraph designs considered for LUVOIR-B. Dashed and dotted lines indicate the contrast (left vertical axis) as a function of angular separation for point sources and resolved stars (0.1 λ/D), respectively. Solid lines indicate the planet throughput (right vertical axis), measured as the encircled energy in a 0.7 λ/D disk, as a function of angular separation. Without a central obscuration the majority of the designs submitted by the community to the LUVOIR team achieve an efficient compromise between robustness to resolved stellar angular size and throughput. Choosing a coronagraph for an off-axis telescope then consists of trading yield vs technological maturity. C. Stark (STScI), G. Ruane (JPL), R. Belikov (NASA Ames), D. Sirbu (NASA Ames).

3.5.2 Component level maturity

The manufacturing of PIAA aspheric optics has progressed considerably over the past few years. Early on difficulties were driven by the high curvature regions on the edge of the pupil, where the required apodization was strong. The introduction of pre- and post-apodizers,[50] as well as constraints on the maximum curvature in the prescription of the apodization function,[36] largely addressed this issue. Such improvements in aspheric optics manufacturing are summarized in Kern et al.[51] This publication also showed that contrast limits stem from the manufacturing of complex FPMs instead of aspheric optics manufacturing. As a result, the PIAA LUVOIR designs rely only on opaque FPMs, whose manufacturing is similar to the APLC FPMs. While not included in the baseline of the ECLIPS visible channel, the aspheric mirrors can be designed to replace the off-axis parabolas before and after the FPM.

3.6 Hybrid Lyot Coronagraph

3.6.1 Design

HLCs are the descendants of the Band Limited Coronagraphs,[52] that have historically produced some of the deepest measured contrasts in relevant testbeds conditions.[53] Since then, their design has evolved from a purely grayscale focal plane mask, to optimizing phase and DM shapes. In the case of WFIRST they have been shown to be robust to pointing jitter and to central obscuration/secondary structure[54] (albeit at a cost in throughput). The performance of these designs proposed for LUVOIR are shown in Figs. 5 for LUVOIR A.

3.6.2 Maturity

HLC designs for monolithic telescopes have been tested in vacuum for more than a decade now.[53] Since this technology was selected for the WFIRST CGI instrument it has been tested with an obscured aperture, in static[55] and dynamic environments.[31] Steady progress towards demonstration of 10^{-9} contrast in a relevant environment has been occurring under the context of WFIRST CGI. The manufacturing of the masks for WFIRST is based on dielectric coating of a semi-transmissive spot.

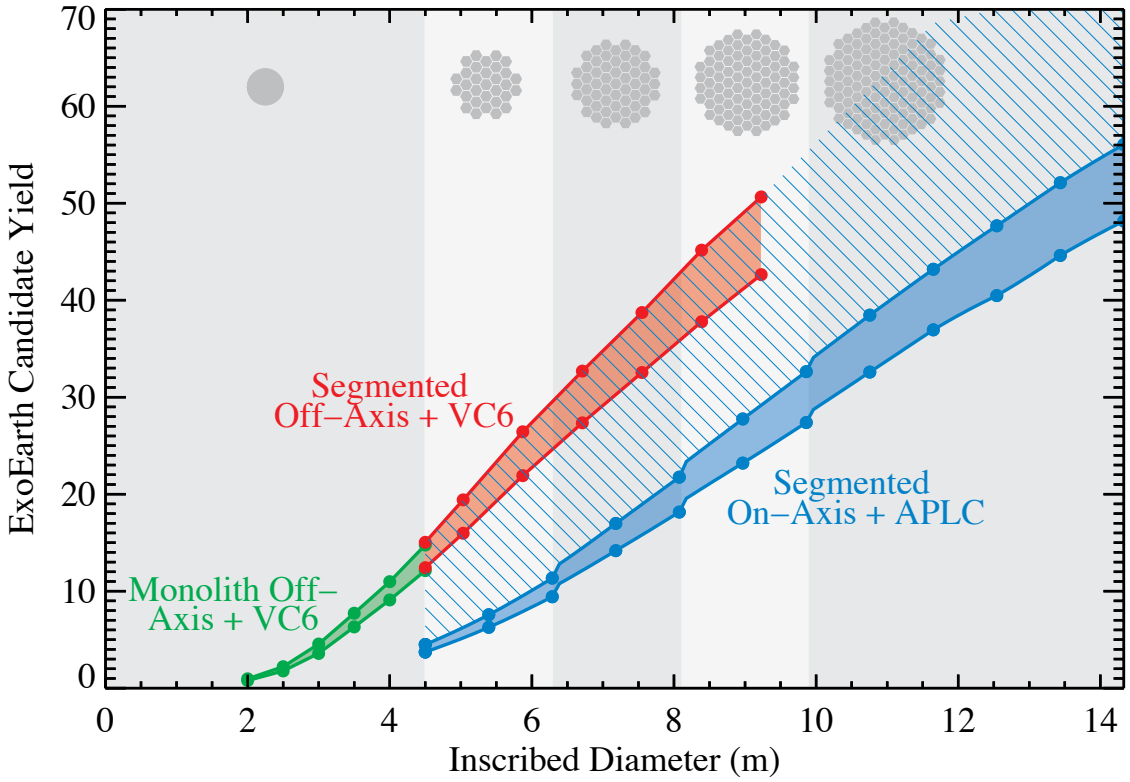

Figure 7: Exoearth candidates yield as a function of aperture, empirically derived using the coronagraph prescriptions discussed in Section 3 and Figs. 5-6. See Stark et al.[5] for underlying assumptions. The introduction of segmentation does not have a strong influence since it can be largely addressed with DMs. On the other hand, because of the high sensitivity of coronagraphs with small IWA to stellar angular size in the presence of central obscurations, on-axis designs have a lower yield than off axis designs. Credit C. Stark (STScI).

3.7 Selected apertures and design

3.7.1 Design trades

All coronagraph technologies yield a level or starlight suppression of at least one part in ten billion (10^{-10}), for all types of apertures. Segmentation by itself has a minor impact on coronagraph performances for all families of coronagraphs, as long as segment gap size is kept small. APLC solutions currently appear relatively insensitive to obscurations, having a similar planet throughput as a function of separation and robustness to stellar angular size. Fig. 5 shows that non-APLC coronagraph designs considered by the LUVOIR do exhibit significant sensitivity to stellar angular size when working with an on-axis aperture. LUVOIR-A's large aperture requires that it be on-axis and thus obscured, since making it off-axis would result in unrealistically large primary-secondary mirror distances and sunshade sizes. As a result the binary APLC coronagraph was selected for this architecture. In this case, aperture size makes up for lower throughput and larger IWA.

For the smaller 8 m LUVOIR-B, the expected exoplanet yield of an on-axis telescope with an APLC coronagraph was deemed too low. By opting for an off-axis telescope with no secondary mirror obscuration, more aggressive coronagraph designs are available. These more aggressive designs partially compensate for the smaller 8 m aperture. Figs. 6 illustrate the performance of Vortex and PIAA coronagraphs for LUVOIR-B. For these two designs segment gaps are corrected using DMs.[37–41] We studied the yield of all possible options,[23] and we baselined the vortex coronagraph as the best trade between technology readiness and scientific return.

A key result of this work was to anchor the quantitative relationship between science return (measured in number of detected exoEarth candidates) and telescope aperture[56] with realistic coronagraph designs and

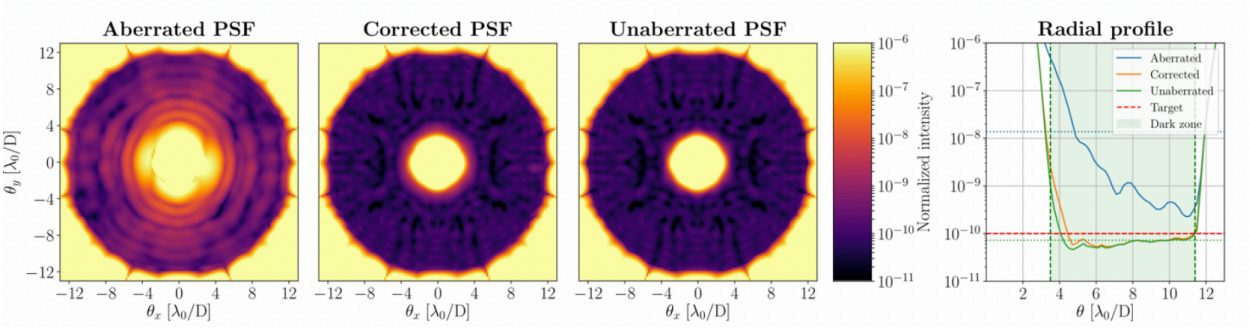

Figure 8: Simulations of static wavefront control: correcting the intrinsic differential polarization of the LUVOIR A design with the DMs in ECLIPS, from Will et al. in these proceedings. From left to right: aberrated coronagraph response in the presence of differential polarization error, corrected response with DMs on, perfect response in the absence of aberrations, radial profiles. Credit S. Will (U. Rochester).

simulations. This result is shown in Fig. 7 and was already presented in Stark et al.[5] Here we briefly remind the reader of the key features of today's exoEarth yield landscape:

• Since DMs can generally correct for segments gaps, there is no significant penalty for going from a monolithic to a segmented aperture.

• For obscured apertures, most state-of-the-art coronagraphs still exhibit strong coupling between IWA, throughput, and robustness to stellar angular size. As a result there is a penalty in yield for switching to on-axis telescope designs, since the only coronagraph robust enough on such apertures has modest throughput.

• These limitations do not stem from fundamental physical properties of diffraction. As a matter of fact, an "ideal" coronagraph, shown in Fig. 5, does not feature these limitations. Future work will improve upon the work presented on Fig. 7.

3.8 Static contrast

Each channel has two DMs, for amplitude and phase wavefront correction. In order to fully take advantage of the degrees of freedom provided by such a layout with respect to i)correctable spatial frequencies[57] ii) contrast/throughput,[40,41] we have baselined DM technologies with a small actuator pitch. Since the optimal operating point scales as D^2/z (z being the distance between DMs) we decided to choose small DMs diameters in order to keep the optical layout compact enough. This drove our choice to baseline MEMS-based DMs.[58] High density (1000+ actuators) DM technologies, capable of repeatable motions at the picometer resolution, are a major component level risk for coronagraphs in space. We refer the readers to the discussions in[58–60] for descriptions of the readiness of these technologies. Here we assume that the demonstration in,[53] combined with future flight projects (either with small satellites[61] or WFIRST-CGI, will serves as a robust enough proof of concept for LUVOIR.

The static wavefront errors/misalignments will be removed by the DMs[53,62,63] using diagnostics based on post-coronagraph images. Overall limitations in the instrument bandpass stem from the chromatic limitations of static wavefront control,[9] rather than from the coronagraph mask design. However, as long as the optical surface requirements are adequately constrained,[64,65] the 2-DM control architecture will meet the $\sim$ 20% bandpass specification of the coronagraph masks. The IWA is most often driven by the coronagraph design, while the OWA is set by the either the number of actuators on the DMs or higher order phase to amplitude conversion.[9] Finally, differential polarization, originating from high incidence angles on the telescope's primary, can possible limit the static contrast, just as it was the case for early WFIRST-CGI designs.[66] Simulations using the LUVOIR A and B telescope prescriptions, alongside with static Wavefront Sensing and Control (WFS&C) in ECLIPS, show that the impact of polarization errors is minimal once they have been corrected with DMs Fig. 8.

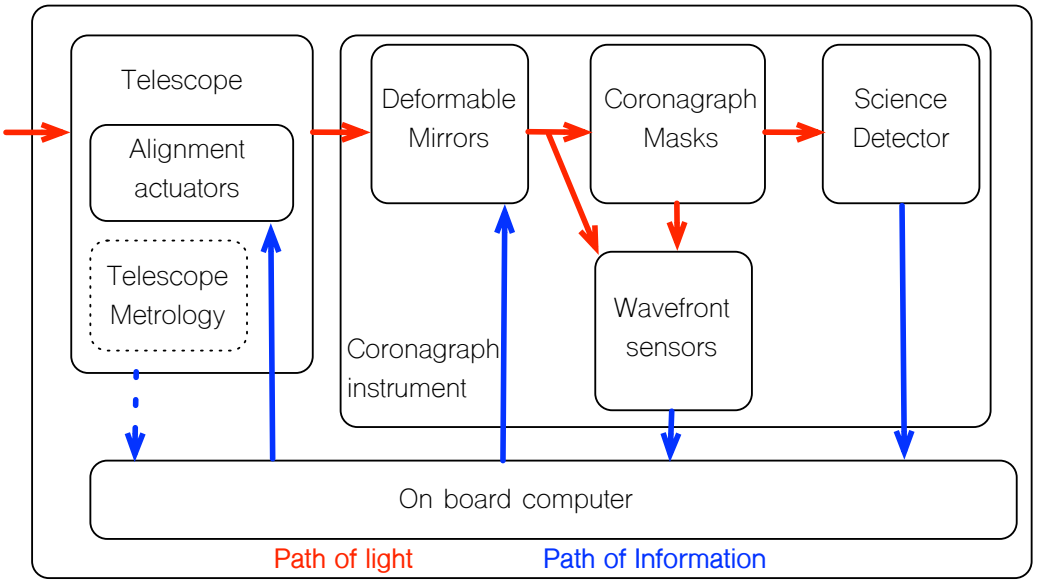

Figure 9: Illustration of the main subsystems needed for ExoEarth imaging from space with a coronagraph. Images at the science camera anchor the Deformable Mirrors (DMs) shapes at the ∼ cadence of science exposures. For faster variations, auxiliary wavefront sensors provide the information needed for DM updates. This information is fundamentally limited by the numbers of photons received from the exoplanets' host stars.

4. WAVEFRONT SENSING AND CONTROL (WFS&C): THE STABILITY PROBLEM

4.1 Optical stability and WFS&C

To maintain a desired contrast, all coronagraphs require stability over a range of spatial scales. Some of these instabilities are filtered out by the static response of the coronagraph,[26,39] some can be controlled/damped at the observatory level, and others can be allowed to vary, with their impact averaging out. However, all coronagraph designs have a range of pathological misalignment modes to which they are very sensitive. To achieve starlight suppression of $\sim 10^{-10}$ over long timescales, pm-level stability must be maintained for these modes and controlled as fast as possible. The solution is to use Deformable Mirrors (DMs) within the coronagraphic instrument, that are used to set the static operating point, to dynamically adjust to correct wavefront error. Their optimal surface settings are based on measurements obtained with a wavefront sensor (WFS). Such a system greatly relaxes requirements on the observatory, since pm stability now must only be maintained for the amount of time it takes to sense and correct the wavefront.

Fig. 9 shows the flow of light and information for a typical WFS&C system. Some of the light is separated from the main science beam and reaches WFS&C channel(s), that calculate the wavefront error in real time on board the telescope, and determine the updates to the DMs (and potentially the telescope). While maintaining pm stability during the WFS cycle is challenging, it is not impossible. The LISA pathfinder mission already demonstrated Optical Path Length (OPL) stabilization that is in principle commensurate with stable starlight rejection of $\sim 10^{-10}$. e-LISA's modern passive dampers along with a laser-based metrology system limited the relative acceleration between two test masses, separated by 30 cm, all the way down to 10 fm s^{-2}/sqrt(Hz), over timescales ranging from ten seconds to three hours.[67] At timescales of the order of minutes, these performances can be understood as OPL drifts of about five picometers, remarkably close to what is needed for exoEarth imaging in space.[68] Similar measurements have been also carried out for an imaging telescopes in a controlled testbed environment.[69]

4.2 Ground Based ExAO vs space based WFS&C

To date, there has been no end-to-end space-based demonstration of a telescope + coronagraph system that operates at the few parts in ten billion rejection level. However, taken independently, the subsystems illustrated on Fig 9 all have a rich history of testing and characterization. These proofs of concept have occurred in a mixture of environments ranging from laboratory experiments to on-sky observations with ground-based adaptive optics systems and the Hubble Space Telescope (HST). Overall, the challenge associated with the coronagraph-based search for life endeavor resides less in the basic technological ingredients, and more in having all of them work together integrated into a complex system with multiple control loops interacting across a range of spatial and temporal scales.

Extreme Adaptive Optics (ExAO). Ground based ExAO instruments routinely take advantage of the architecture in Fig. 9 to yield the image stability necessary to discover young giant planets.[70–75] Because the spatial and temporal scales of atmospheric turbulence are correlated, achieving image stability close to the star requires correcting a larger number of modes faster.[76–78] This significantly increases the system complexity associated with ExAO instruments. This push towards faster systems is one of the key drivers underlying exoplanet imaging instrumentation for Extremely Large Telescopes (ELTs). It will bring to full maturity algorithmic advances such as optimal modal decompositions[79] and predictive[80,81] control and will occur regardless of NASA programmatic decisions. However, future missions will greatly benefit from these innovations. Remaining temporal image variations are subtracted using optimized observation strategies and post-processing algorithms,[82–84] which will also become more sophisticated as ELTs will try to detect planets as close as possible to their host star.[85]

Space-based coronagraphs. Today's generation of space-based coronagraphs do not feature DMs. Instead, it places a premium on making the environment as stable as possible, in a "set and forget" paradigm. HST represents the state or the art, with a stability in a Low Earth Orbit resulting in contrasts at the $\sim 10^{-6}$ level, after post-processing.[86] Models of an improved environment at L2 yields similar performances, at much better resolution and sensitivity, for JWST[87] (albeit at longer wavelengths). WFIRST-CGI simulations predict that a much deeper *static* contrast can be reached once DMs are added.[66] We note that the fundamental coupling between temporal and spatial scales limiting the angular resolution of ground-based observations can be addressed by design for a space-based observatory: the thermal and dynamical response of a space telescope can be engineered better than weather can be controlled. This careful engineering hinges on mechanical and thermal modeling of the observatory (spacecraft + telescope + instruments). Such models plays a key role in predicting the performances of coronagraphs in space.[66,87] They are extremely complex and have never been fully validated against flight hardware, even at the nanometer level, let alone at the picometer level. Recent JWST cryovac thermal tests were a first step towards reconciling observatory integrated models and flight hardware.[87] JWST and WFIRST flight-data will further solidify their fidelity.

"ExAO from space". LUVOIR will rely on auxiliary WFS and DMs to address wavefront stability, a de facto implementation of ExAO in space (see Fig. 9). This choice was driven because of the risk and uncertainties associated with open loop wavefront stability: the "set and forget" observing paradigm hinges on the observatory integrated models to be *exactly* right at the picometer level, with little room for uncertainty factors. In the absence of models validated against flight data, the LUVOIR team chose to rely on continuous WFS&C, even though this has never flown in space. This architecture was deemed a good trade to address the risk associated with making large structures in space ultra stable, with the WFS&C system complexity risk partially retired (albeit at more modest contrasts) by current ExAO instruments.

The envisioned closed-loop operations of ECLIPS flow as follows. The static and very slow errors will be removed by the DMs using diagnostics based on the actual science exposures (see above). Auxiliary wavefront sensors will then provide DM corrections at a cadence faster than the science exposures. Fig. 10 illustrates their modal and temporal response (in frequency space). Such technologies, and their operations, have been matured at ground-based observatories. Future missions need to optimize them in order to reduce the closed-loop residual misalignments from the nanometer scale to the picometer scale. This is exactly what happened for WFIRST CGI: the Zernike WFS was first envisioned and tested for ground based telescopes,[88,89] but quickly adopted and demonstrated in a relevant laboratory environment for WFIRST.[31,90] ExoEarth finding missions will have to control more spatial modes than WFIRST, and will require a more optimized WFS architecture. Thus, the

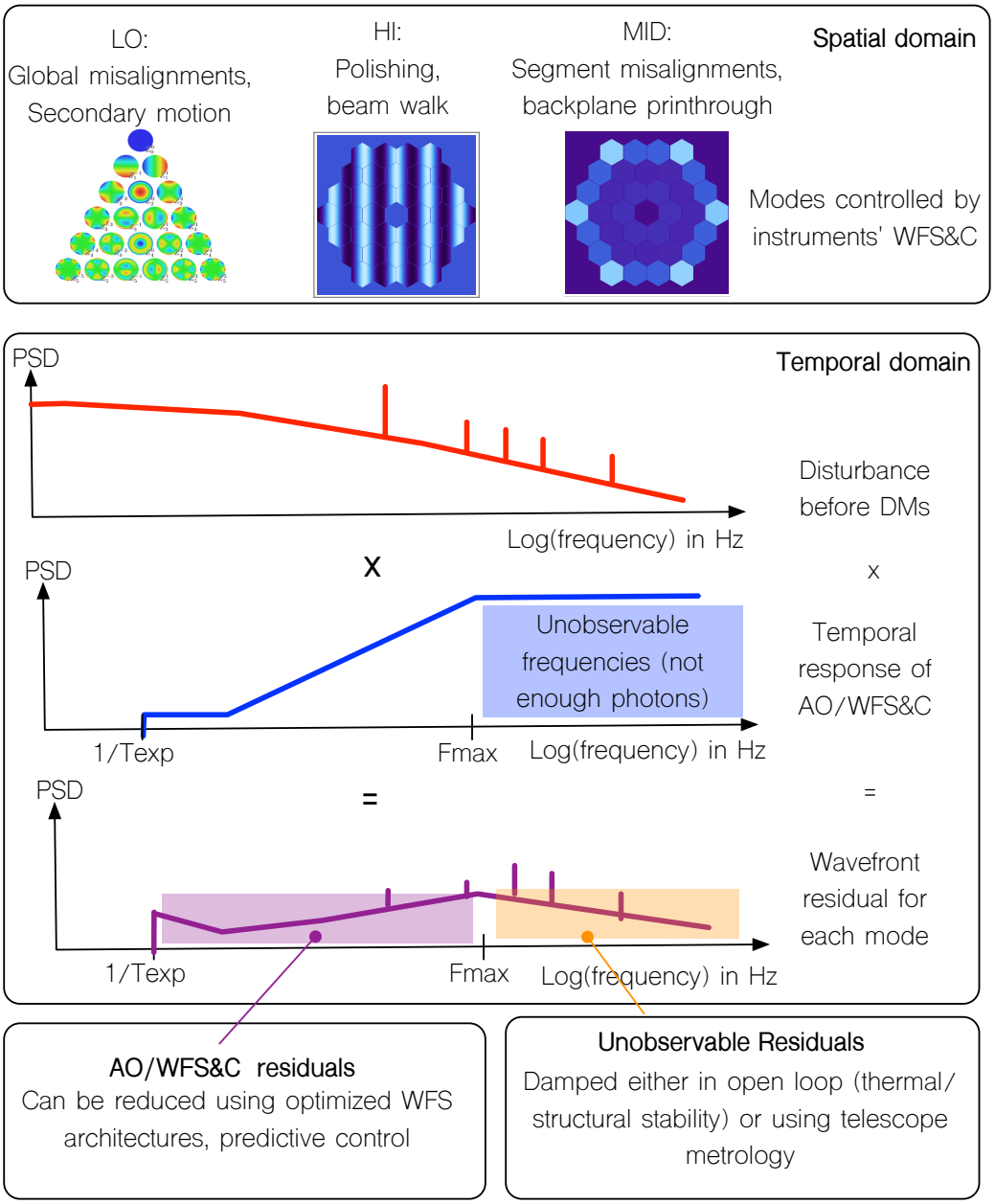

Figure 10: Representation of the instrument WFS&C response in the frequency domain. Above the cutoff frequency F_{Max}, set by the photon noise, telescope imperfections cannot be corrected by the science instrument. If passive structural damping at the observatory level yields residuals above this frequency, an active metrology system is necessary at the observatory level.

LUVOIR ECLIPS concept represents a natural evolution in the the transfer of technology from ground-based ExAO systems to flagship space observatories.

4.3 Spatial and temporal timescales for ECLIPS

4.3.1 Error budgeting principle

In order to understand the requirements on the intrinsic stability of the observatory, and in particular how they can be relaxed with the WFS&C sub-system, we separate the spatial and temporal timescales into different

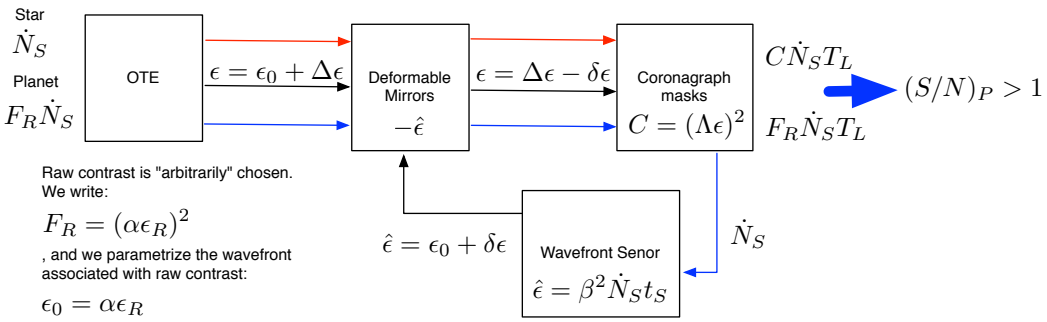

Figure 11: Notations underlying our order of magnitude calculation for wavefront drift requirements.

regimes, as illustrated on Fig. 10. This formalism is inspired by previous work on the JWST error budget[91] and ongoing work on ultra-stable segmented telescope concepts (Coyle et al., in these proceedings).

4.3.2 Spatial scales

We split the spatial timescales as follows:

• LO spatial scales. These modes will arise from global misalignments in the telescope assembly (secondary mirrors misalignments in particular), or potential non-common paths between the science camera and the auxiliary WFS. We describe them as Zernike polynomials. Making static coronagraph designs robust to stellar angular size often also makes them robust to LO modes.

• MID spatial scales. These modes will arise from segment misalignments at the primary (they are not present in a monolithic observatory). Since the primary mirror is the only segmented optic that can create such modes, these modes can be be fully sensed by a sensor after the primary: architecture optimization against non-common path is not necessary for these modes. Both LUVOIR architectures have at least 10 segments across the telescope aperture. As a result the main harmonic associated with MID scales will appear in the middle of the coronagraph dark zone—prime real estate for exoplanet hunting. We treat them using the formalism laid out in Leboulleux et al.[92,93]

• HI spatial scales. These modes will primarily arise from surface polishing errors at high spatial frequencies. Most of them are static. However cross talk between LO modes and the static DM solutions (such as jitter-induced beam walk) can introduce HI modes at the entrance of the coronagraph. We treat them as sinusoidal ripples since they have been described as such over the past couple of decades.

If each mode is independent (that is their cross term is zero in intensity), then the instantaneous contrast is directly tied to the sensitivity of the static coronagraph design to a given mode. This is true by construction for all modes within each one of the LOW, MID, HI regimes, and we assume that it is also true across regimes. Future work will include these nonlinear cross-terms.

4.3.3 Timescales

There are two types of excitations that can create time varying wavefront errors: thermal, with drifts ranging from a few minutes to hours[87] and mechanical, with frequencies as fast as $10 - 100$ Hz. There also are two key timescales driving the temporal response of the coronagraph instrument: the exposure time T_L, and the shortest possible time between DMs updates t_s. The former timescale is chosen based on the host star brightness during the DRM. T_L is set so that the noise floor (photon noise in the image) associated with a given level of static starlight extinction (or raw contrast) is small enough to detect exoplanets at sufficient SNR. The latter timescale is driven by the time it takes to sense a fixed wavefront given the limited number of photons available for sensing (limited by the stellar magnitude). If we think of the WFS&C system as a temporal high pass filter, as shown on Fig. 10, this timescale is inversely proportional to its cutoff frequency $t_s \sim 1/F_{Max}$.

The regimes depending on the exposure time are:

• When the timescale of a given range of spatial modes is much shorter than the science exposure time, and the modes de-correlate over the course of an exposure (that is the relative power in the modes changes fast

enough), then then these modes average as a uniform halo in the coronagraph images. This halo can be removed in post-processing via spatial filtering and thus the limiting quantity for exoplanet detection is the shot noise associated with this halo.

• When the timescale of a given range of spatial modes is of the same order of the exposure time, then the coronagraph images have structures (these are also called "speckles"). These noise artifacts look like copies of an actual exoplanets. They either need to be small enough so that exoplanets are detected at sufficient SNR, or image subtraction (using reference stars for instance) is needed. Under the latter scenario, the change in wavefront need to be small enough during the course of the science exposure (and the change in observatory configuration if reference observations are used) so that the noise after post-processing is low enough. This regime is equivalent to the the case of a timescale much shorter than the exposure time with the relative power in each modes remaining correlated.

In the absence of an auxiliary wavefront sensor, the only relevant timescale is the science exposure time. With an auxiliary wavefront sensor, there are two regimes of wavefront error timescales to consider:

• Below $1/F_{Max}$: In the presence of auxiliary wavefront sensors that provide DM corrections at a cadence faster than the science exposure, the fundamental lower bound on wavefront correction time, $\sim 1/F_{Max}$, depends upon host star brightness and WFS architecture. When incident wavefront errors are slower than $\sim 1/F_{Max}$, the contrast residual is driven by the residual noise in the control loop, which scales as the shot noise in the WFS.

• Above $1/F_{Max}$: When incident wavefront errors vary faster than $\sim 1/F_{Max}$, we assume that they are not corrected (in practice they might partially corrected) and they directly impact the science images, as if there was no WFS&C.

Table 1: Order of magnitude estimates of the wavefront drift requirements for LUVOIR B. For these calculations we consider a raw static contrast of 10^{-10}, a planet to star flux ratio of 10^{-11}, a $m_V = 5$ star, and assumed that the closed-loop residuals for LOWFS and OBWFS are both driven by the shot noise in the wavefront sensor. Requirements for LUVOIR A have a similar order of magnitude: in that case the increase in photon counts compensates the degradation in robustness to misalignments.

Quantity	**Expression**	**HI modes**	**MID modes**	**LO modes**
Drift requirement without WFS&C	$\frac{1}{SNR_P^3}\frac{\dot{N}_S F_R^{3/2}}{2\alpha^3\Lambda}$	0.04 pm/10 hrs	2 pm/10 mntss	50 pm / 10 hrs
Drift requirement with WFS&C	$\frac{1}{SNR_P^3}\frac{\dot{N}_S F_R^{3/2}}{2\alpha\beta^2\Lambda^3}$	1 pm/10 mnts	500 pm/10 mnts	50 nm/10 mnts
Largest correctable temporal frequency	$\frac{\dot{N}_S}{\beta^2\Lambda^2(SNR)_P^2}$	0.03 Hz	0.2 Hz	2 Hz
Integrated temporal PSD of fast varying uncorrected and uncorrelated modes	$\int_{F_{max}}^{+\infty} \widehat{\lvert\epsilon(\nu)\rvert^2} d\nu$	10 pm	30 pm	100 pm

4.3.4 Drift requirements

For a given flux ratio between the star and the planet, we use a simplified analytical approximation to derive the drift requirements for each spatial mode. These requirements vary depending on our assumptions regarding observing scenarios and data processing. Since there are numerous options, we limit ourselves here to "one to one" differential imaging (e.g., there is a reference star before or after science observations) using high pass filtering to remove a potential halo. We consider the cases with and without WFS&C during the science exposure. Applying the same notations as Fig. 11, the largest wavefront change possible so that a planet is detected after differential imaging can be written as $\Delta\epsilon \sim \frac{\sqrt{F_R}}{2\alpha\Lambda(SNR)_P}$. This assumes that the science exposure is long enough to beat the shot noise in the raw data: the shortest science exposure time required to achieve this is $T_L \sim \frac{(SNR_P)^2\alpha^2}{\dot{N}_S F_R}$. The shortest WFS exposure time given stellar photon arrival rate and WFS architecture is

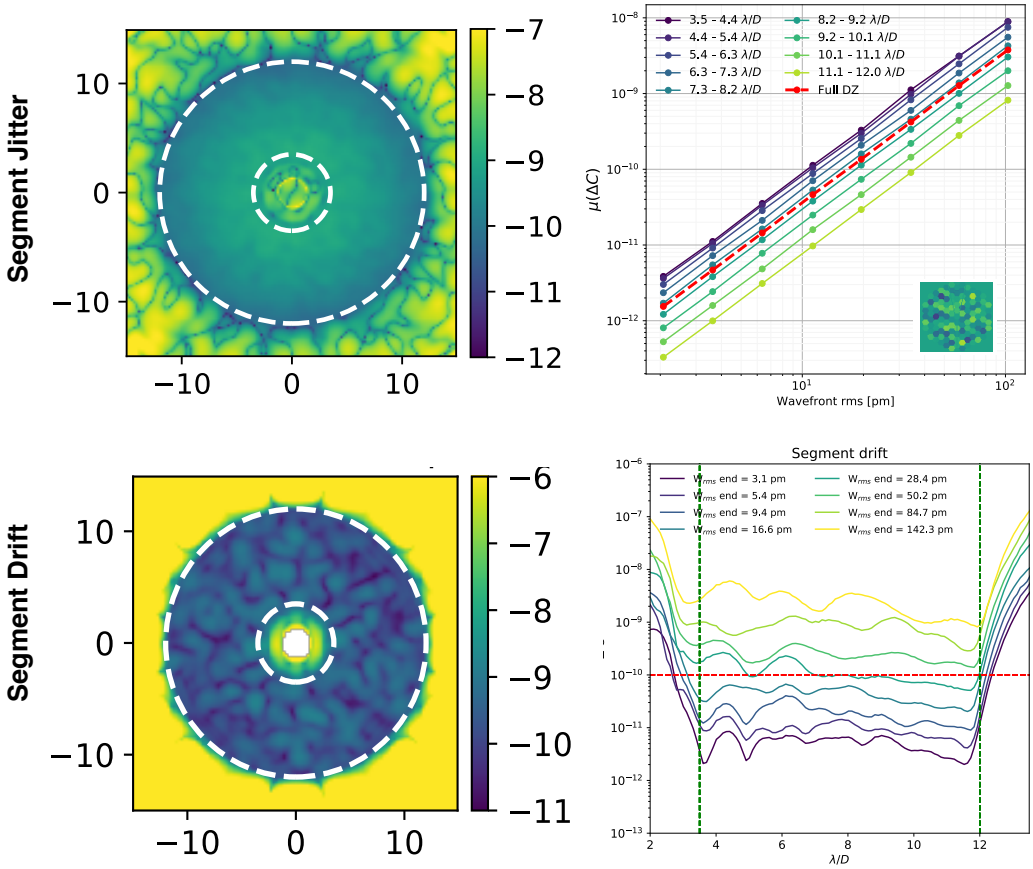

Figure 12: Sensitivity of the LUVOIR A ECLIPS coronagraph design to generic MID modes. Top left: Coronagraph response to random segment jitter. Top right: contrast as a function of segment jitter amplitude. Bottom left: Coronagraph response to systematic segment drift. Bottom right: contrast as a function of segment drift amplitude. Credit R. Juanola-Parramon (GSFC), N. Zimmerman (GSFC).

$t_s \sim \frac{\beta^2 \Lambda^2 (SNR)_P^2}{\dot{N}_S} \sim 1/F_{Max}$. Under the assumption that drift requirements can be expressed as a simple upper limit over the wavefront time derivative, the requirements under the set-and-forget scenarios can be written as $d_{SF} \sim \Delta\epsilon/T_L$ and the ones under continuous WFS as $d_{WFS} \sim \Delta\epsilon/t_S$. Table. 1 summarizes the requirements for LUVOIR-B using under these two hypothesis. Here we stress that these calculations are not a substitute for detailed WFS&C simulations, they are merely an order of magnitude initial error budget that illustrates potential gains associated with implementing WFS&C on LUVOIR. However, we have checked that our analytical approach does yield results commensurate to the previous publications (within a factor of ~ 2), that carried out detailed simulations for a subset of spatial and temporal regimes.[94–96]

WFS&C relaxes the requirements for drifts slower than F_{max} by a factor that scales as the inverse of the raw contrast ($1/\alpha$), the WFS efficiency (β) and the coronagraph sensitivity to a given mode ($1/\lambda$). The value of raw contrast is set by coronagraph design and static WFS&C. The deeper it is, the less sensitive to time varying drifts the system will be. The other two parameters, sensitivity to misalignments and wavefront sensing efficiency, also play an important role in the exoplanet detection capabilities of ECLIPS, and have only been recently included in testbed experiments. The design of ECLIPS takes full advantage of these two lever arms to reduce the risk associated with optical stability. For any type of coronagraph, sensitivity to HI modes cannot be reduced without severely hampering the planet throughput, since both they both feature the same morphology. On the other hand, making the mask designs robust to stellar angular size automatically reduces the sensitivity to LO and MID modes. Should further modal attenuation in the MID regime be needed, it can be in principle be

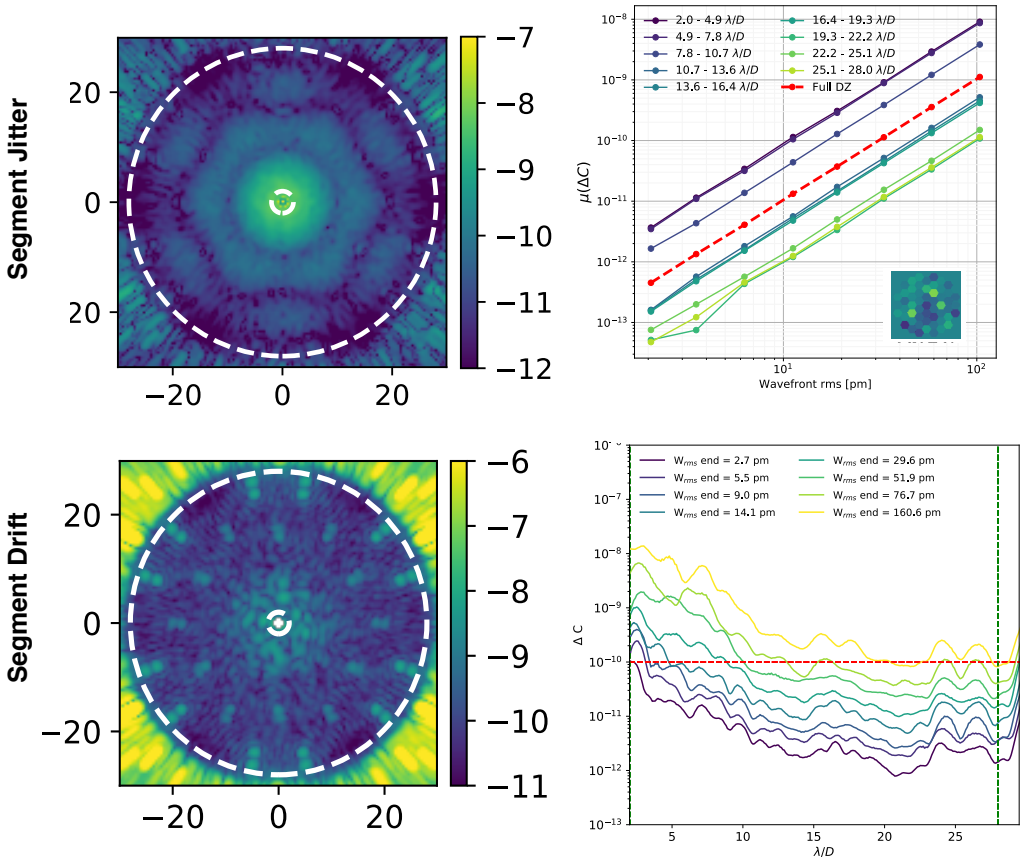

Figure 13: Sensitivity of the LUVOIR-B ECLIPS coronagraph design to generic MID modes. Top left: Coronagraph response to random segment jitter. Top right: contrast as a function of segment jitter amplitude. Botton Left: Coronagraph response to systematic segment drift. Bottom right: contrast as a function of segment drift amplitude. Credit R. Juanola-Parramon (GSFC), N. Zimmerman (GSFC).

included as an explicit constraint in the mask optimization problem. The sensitivities to MID modes are shown on Figs. 12-13, from Juanola-Parramon et al. in these proceedings. Next we discuss how the Wavefront Sensing architecture of ECLIPS was designed in order not maximize photon efficiency.

4.4 WFS architectures for ECLIPS

4.4.1 Instrument based WFS&C

The WFS architecture in ECLIPS will be key to minimizing residual starlight and thus relaxing the requirements on the stability of the LUVOIR observatory. This implies estimating the fastest wavefront variations possible with sufficient SNR. As a result, an optimal WFS should:

• receive as many stellar photons as possible. This is achieved by capturing the starlight that is rejected from the coronagraph masks by designing masks as "beamsplitters".

• minimize the number of optics in the science channel after the WFS pick-off (also called Non-Common Path, NCP). If such optics get misaligned on timescales faster than the science exposure, then the associated image artifacts cannot be sensed and corrected.

• efficiently convert nanometers of misalignment into intensity variations that can be sensed by a detector. This is quantified using a scalar number, called WFS efficiency that relates WF error and the measurement's photon noise.[70, 78]

Under these guiding principles the ECLIPS instrument is equipped with both Low-Order and Out-of-Band WFS (LOWFS and OBWFS, respectively).

• The OBWFS[94] will use one of the three coronagraph channels for sensing the segment motions of the primary, while the other two are being used for science integrations. A Zernike phase mask[88] has been baselined in the focal planet wheel of each coronagraph channel for this purpose. This architecture features a fair amount of non-common path errors, however only has a small impact on final performances since MID errors do not arise downstream of the primary mirror. OBWFS can also be used for HI errors.

• The LOWFS will use the light rejected by the coronagraph in each channel to sense the LO modes. Because those can arise in internal instrument optics the sensing architecture need to minimize non-common path errors, with the light picked off at the focal plane mask of the binary APLC[31] or at the Lyot plane for the vortex coronagraph.[97] The phase to intensity modulation is then obtained using a Zernike phase mask.[88]

• Both the OBWFS and LOWFS use the bulk of the starlight received by the telescope, which, combined with the Zernike mask, makes then very photon efficient ($\beta \sim 1$). Using the data from science camera to maintain optimal DM shapes,[98,99] on the other hand, requires much longer exposures since it only receives a fraction of the starlight. However, a science camera-based WFS is a promising avenue to maintain the absolute DM solution during long observing sequences and is the only sensing architecture that can update the HI modes. Since it does not require extra hardware, it has also been baselined by LUVOIR.

4.4.2 Observatory based WFS&C

For the disturbances with timescales that are faster than what can be corrected using instrument-based WFS&C, telemetry "at the source" of the disturbance, that does not use the photons from the exoplanet host star to diagnose misalignments, is needed. For the MID modes segment level misalignments can be sensed using edge sensors, that have recently demonstrated sensitivities at the picometer level.[100] LO modes, and in particular global misalignments of the secondary mirror with respect to the rest of the observatory can be sensed with a laser truss.[101,102] Finally, all spatial scales can be sensed using a laser guide star at a much faster rate than relying only on the target star's light.[95] High speed interferometric techniques are now sensitive, in open loop, to sub-picometer displacements.[69] Whether any or all of these techniques are required for ECLIPS observations with LUVOIR A or B depends on the performances of instrument-based WFS&C (and in particular how large F_{Max} can be) and the temporal content of the observatory disturbances. This very specific question is currently being investigated in an effort parallel to the LUVOIR study, with preliminary results presented by Coyle et al. in these proceedings. While more detailed work is required here, we qualitatively discuss our current understanding of each spatial regime:

• LO modes: current WFIRST simulations show that only the first three or four LO modes vary significantly over the course of a science observing sequence.[31] LUVOIR, on the other, will feature much larger opto-mechanical structures and thus be more sensitive to fast dynamics-driven instabilities. This is mitigated by the facts that a) the LUVOIR coronagraphs have been designed to be fairly insensitive to LO modes, b) the large aperture allows faster wavefront sensing (large F_{Max}). As a result, it is not clear yet if a laser truss to sense LO modes at fast timescales is needed, however the LUVOIR team has conservatively included such hardware in LUVOIR A and B.

• HI modes: these modes arise mostly from manufacturing errors and thus do not change with time. However, second order phenomena, such as pointing jitter-induced beam walk can introduce HI modes at fast timescales (faster than F_{max}). Mitigation strategies include observatory level HI modes telemetry and/or controlling beam walk at the source, with a Fast Steering Mirror (FSM) before ECLIPS. The LUVOIR designs include such a FSM. However, future work is necessary to reduce the line-of-sight residuals below the levels for which beam walk will be negligible.

• MID modes: Both LUVOIR A and B have baselined segmented primary mirrors equipped with edge sensors[101] in order to sense the variations in MID modes at timescales faster than F_{max}. Interestingly, the main limitations of these components are in long-term bias drifts, that can be handled by the instrument-based WFS&C. Ongoing work is currently conducted to make sure that the critical timescales of both sub-systems overlap.

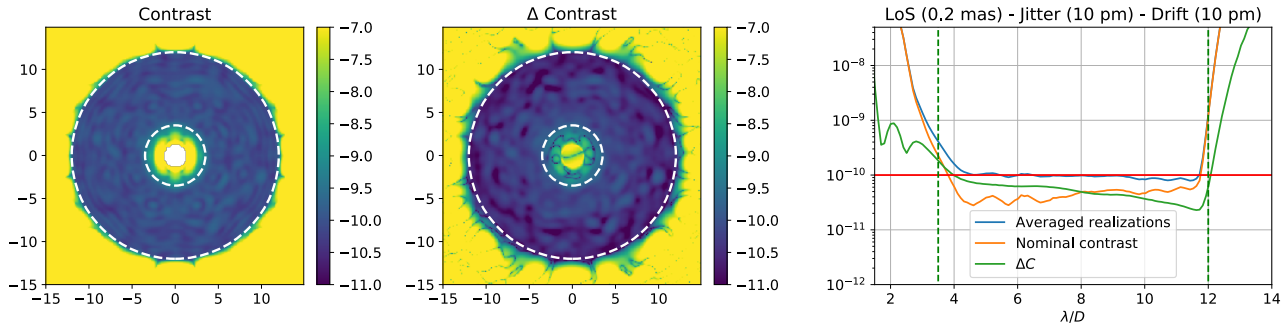

Figure 14: End-to-end simulations of a differential imaging observing sequence with ECLIPS A, assuming 10 *pm of uncorrelated MID modes random variations,* 10 *pm of correlated MID modes drifts over the course of the observation, and* 0.2 *mas of residual line-of-sight pointing jitter. If the wavefront can be stabilized to these levels, using a combination of instrument- and observatory-based WFS&C then the noise floor associated with wavefront instabilities is of the same order as the one associated with the static instrument design. Credit R. Juanola-Parramon (GSFC), N. Zimmerman (GSFC).*

The overall complexity of the observatory-level WFS&C scales as the inverse of the fastest temporal frequency correctable with instrument-based WFS&C. Ground-based ExAO systems also face the challenge of having to run as fast as possible with a finite WFS photon noise floor set by the host star. Because they need the effective IWA to be able to image temperate planets around nearby stars, they have to operate with F_{max} as large as possible.[78] This warrants extremely fast calculations.[103,104] While the actual hardware would be dramatically different for space-based applications (that do not require $> kHz$ correction frequencies), algorithmic advances from the ground-based community, including predictive control algorithms, can be readily applied to exoEarth finding missions.[80,81] As a matter of fact, predictive control algorithms have already been used on space technology testbeds[98,105,106] and have recently been used to demonstrate that requirements on the observatory beyond the photon noise limit are possible[99] (de facto making $\beta < 1$).

4.4.3 Simulations

As of today there are no integrated structural-thermal-optical performance (STOP) models of LUVOIR with ECLIPS operating in conjunction with WFS&C at all relevant spatial and temporal scales. Such simulations will be critical to refine the error budget and WFS&C architecture beyond what we presented here. Even in the absence of such large-scale numerical models, there is already a large body of work of simulations focusing on one or a few sub-systems/scales.[94–96,102,107] Based on these published results we have conducted LUVOIR ECLIPS simulations assuming 10 pm of uncorrelated MID modes random variations, 10 pm of correlated MID modes drifts and 0.2 mas of line of sight jitter, all of them over the course of a science exposure. Details for these simulations can be found in the proceedings, in Juanola-Parramon et al. Figures 14 and 15 show that differential imaging under these assumptions yields a contrast floor below the nominal 10^{-10} raw contrast of the static coronagraph design. Future work needs to establish with more granularity which combination of all the WFS&C sub-systems has conservatively baselined is a viable architectures to provide $\sim$ 10 pm residuals after DM correction. Future testbed demonstrations will then need to establish such closed-loop residuals experimentally.

5. CONCLUSION

In this paper we have presented the trades underlying the design of the Extreme Coronagraph for Living Planetary Systems (ECLIPS) instrument of the LUVOIR Mission Concept. ECLIPS is one of the most ambitious exoplanetary science instruments ever proposed, and we strove to find the optimal balance between performance and technological maturity. This paper presents the point design of the LUVOIR Study Team circa August 2019. Since both exoplanetary science and coronagraph technology are dynamic fields of research, instrument concepts for imaging exoEarths with future space observatories are bound to evolve along with their advances.

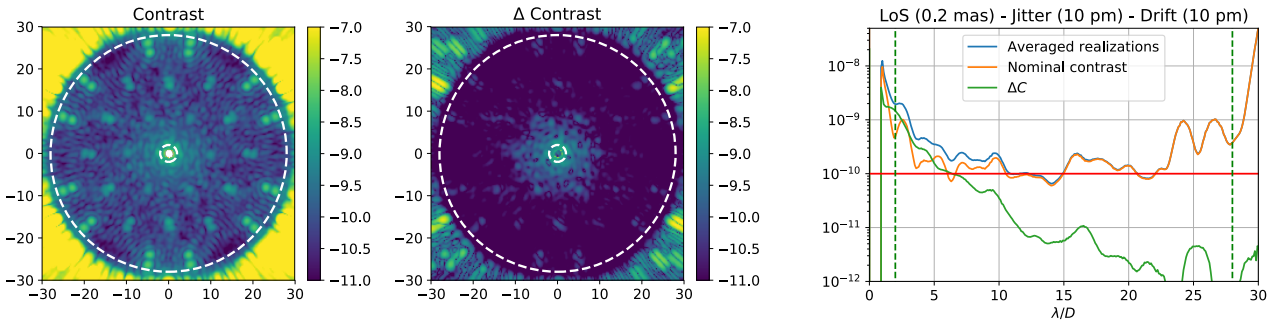

Figure 15: End to end simulations of a differential imaging observing sequence with ECLIPS B, assuming 10*pm of uncorrelated MID modes random variations,* 10*pm of correlated MID modes drifts over the course of and* 0.2 *mas of line of sight jitter. If the wavefront can be stabilized to these levels, using a combination of instrument and observatory based WFS&C then the noise floor associated with wavefront instabilities is of the same order as the one associated with the static instrument design. Credit R. Juanola-Parramon (GSFC), N. Zimmerman (GSFC).*

ACKNOWLEDGMENTS

This work was supported by the LUVOIR Mission Concept Study Team. More details can be found in LUVOIR Final Report, $https://asd.gsfc.nasa.gov/luvoir/resources/docs/LUVOIR-FinalReport-2019-08-26.pdf$. A portion of this research was carried out at the Jet Propulsion Laboratory, California Institute of Technology, under government contract. This work is supported in part by the National Aeronautics and Space Administration under Grants NNX12AG05Gand NNX14AD33G issued through the Astrophysics Research and Analysis (APRA) program (PI: R. Soummer) and by Jet Propulsion Laboratory subcontract No.1539872 (Segmented Aperture Coronagraph Design and Analysis; PI: R. Soummer). The design of the ideal and PIAA coronagraphs in this work was supported in part by the NASA Ames Research Center and by the Strategic Astrophysics Technology / Technology Development for Exoplanet Missions (SAT/TDEM) program through solicitation NNH16ZDA001N-SAT at NASA's Science Mission Directorate. It was carried out at the NASA Ames Research Center. Any opinions, findings, and conclusions or recommendations expressed in this article are those of the authors and do not necessarily reflect the views of the National Aeronautics and Space Administration.

REFERENCES

[1] of Sciences Engineering, N. A. and Medicine, [*Exoplanet Science Strategy*], The National Academies Press, Washington, DC (2018).

[2] Gaudi, B. S., Seager, S., Mennesson, B., Kiessling, A., Warfield, K., Kuan, G., Cahoy, K., Clarke, J. T., Domagal-Goldman, S., and Feinberg, L., "The Habitable Exoplanet Observatory (HabEx) Mission Concept Study Interim Report," *arXiv e-prints* , arXiv:1809.09674 (Sep 2018).

[3] The LUVOIR Team, "The LUVOIR Mission Concept Study Interim Report," *arXiv e-prints* , arXiv:1809.09668 (Sep 2018).

[4] N'Diaye, M., Soummer, R., Pueyo, L., Carlotti, A., Stark, C. C., and Perrin, M. D., "Apodized Pupil Lyot Coronagraphs for Arbitrary Apertures. V. Hybrid Shaped Pupil Designs for Imaging Earth-like planets with Future Space Observatories," *The Astrophysical Journal* **818**, 163 (Feb. 2016).

[5] et al., S., "Exoearth yield landscape for future direct imaging space telescopes," *Journal of Astronomical Telescopes, Instruments, and Systems* **5**(2), 1 – 20 – 20 (2019).

[6] Sing, D. K., Fortney, J. J., Nikolov, N., Wakeford, H. R., Kataria, T., Evans, T. M., Aigrain, S., Ballester, G. E., Burrows, A. S., Deming, D., Désert, J.-M., Gibson, N. P., Henry, G. W., Huitson, C. M., Knutson, H. A., Etangs, A. L. d., Pont, F., Showman, A. P., Vidal-Madjar, A., Williamson, M. H., and Wilson, P. A., "A continuum from clear to cloudy hot-jupiter exoplanets without primordial water depletion," *Nature* **529**, 59 EP – (12 2015).

[7] Burningham, B., Marley, M. S., Line, M. R., Lupu, R., Visscher, C., Morley, C. V., Saumon, D., and Freedman, R., "Retrieval of atmospheric properties of cloudy L dwarfs," *MNRAS* **470**, 1177–1197 (Sep 2017).

[8] Feng, Y. K., Robinson, T. D., Fortney, J. J., Lupu, R. E., Marley, M. S., Lewis, N. K., Macintosh, B., and Line, M. R., "Characterizing Earth Analogs in Reflected Light: Atmospheric Retrieval Studies for Future Space Telescopes," *Astronomical Journal* **155**, 200 (May 2018).

[9] Mazoyer, J. and Pueyo, L., "Fundamental limits to high-contrast wavefront control," in [*Society of Photo-Optical Instrumentation Engineers (SPIE) Conference Series*], *Society of Photo-Optical Instrumentation Engineers (SPIE) Conference Series* **10400**, 1040014 (Sep 2017).

[10] Groff, T. D., Mejia Prada, C., Cady, E., Rizzo, M. J., Mandell, A., Gong, Q., McElwain, M., Zimmerman, N., Saxena, P., and Guyon, O., "Wavefront control methods for high-contrast integral field spectroscopy," in [*Society of Photo-Optical Instrumentation Engineers (SPIE) Conference Series*], *Society of Photo-Optical Instrumentation Engineers (SPIE) Conference Series* **10400**, 104000Q (Sep 2017).

[11] Nemati, B., Effinger, R., Demers, R., Harding, L., Morrissey, P., Bush, N., Hall, D., and Skottfelt, J., "The effect of radiation-induced traps on the WFIRST coronagraph detectors," in [*High Energy, Optical, and Infrared Detectors for Astronomy VII*], *Procs SPIE* **9915**, 99150M (Aug. 2016).

[12] Nemati, B., "Detector selection for the WFIRST-AFTA coronagraph integral field spectrograph," in [*Space Telescopes and Instrumentation 2014: Optical, Infrared, and Millimeter Wave*], *Procs SPIE* **9143**, 91430Q (Aug. 2014).

[13] Hinkley, S., Oppenheimer, B. R., Brenner, D., Parry, I. R., Sivaramakrishnan, A., Soummer, R., and King, D., "A new integral field spectrograph for exoplanetary science at Palomar," in [*Proceedings of the SPIE*], *Proceedings of the SPIE* **7015**, 32 (July 2008).

[14] Mawet, D., Ruane, G., Xuan, W., Echeverri, D., Klimovich, N., Randolph, M., Fucik, J., Wallace, J. K., Wang, J., Vasisht, G., Dekany, R., Mennesson, B., Choquet, E., Delorme, J.-R., and Serabyn, E., "Observing Exoplanets with High-dispersion Coronagraphy. II. Demonstration of an Active Single-mode Fiber Injection Unit," *ApJ* **838**, 92 (Apr. 2017).

[15] Hinkley, S., Pueyo, L., Faherty, J. K., Oppenheimer, B. R., Mamajek, E. E., Kraus, A. L., Rice, E. L., Ireland, M. J., David, T., Hillenbrand, L. A., Vasisht, G., Cady, E., Brenner, D., Veicht, A., Nilsson, R., Zimmerman, N., Parry, I. R., Beichman, C., Dekany, R., Roberts, J. E., Roberts, Jr., L. C., Baranec, C., Crepp, J. R., Burruss, R., Wallace, J. K., King, D., Zhai, C., Lockhart, T., Shao, M., Soummer, R., Sivaramakrishnan, A., and Wilson, L. A., "The Andromedae System: New Constraints on the Companion Mass, System Age, and Further Multiplicity," *The Astrophysical Journal* **779**, 153 (Dec. 2013).

[16] Macintosh, B., Graham, J. R., Barman, T., De Rosa, R. J., Konopacky, Q., Marley, M. S., Marois, C., Nielsen, E. L., Pueyo, L., Rajan, A., Rameau, J., Saumon, D., Wang, J. J., Patience, J., Ammons, M., Arriaga, P., Artigau, E., Beckwith, S., Brewster, J., Bruzzone, S., Bulger, J., Burningham, B., Burrows, A. S., Chen, C., Chiang, E., Chilcote, J. K., Dawson, R. I., Dong, R., Doyon, R., Draper, Z. H., Duchêne, G., Esposito, T. M., Fabrycky, D., Fitzgerald, M. P., Follette, K. B., Fortney, J. J., Gerard, B., Goodsell, S., Greenbaum, A. Z., Hibon, P., Hinkley, S., Cotten, T. H., Hung, L.-W., Ingraham, P., Johnson-Groh, M., Kalas, P., Lafreniere, D., Larkin, J. E., Lee, J., Line, M., Long, D., Maire, J., Marchis, F., Matthews, B. C., Max, C. E., Metchev, S., Millar-Blanchaer, M. A., Mittal, T., Morley, C. V., Morzinski, K. M., Murray-Clay, R., Oppenheimer, R., Palmer, D. W., Patel, R., Perrin, M. D., Poyneer, L. A., Rafikov, R. R., Rantakyrö, F. T., Rice, E. L., Rojo, P., Rudy, A. R., Ruffio, J.-B., Ruiz, M. T., Sadakuni, N., Saddlemyer, L., Salama, M., Savransky, D., Schneider, A. C., Sivaramakrishnan, A., Song, I., Soummer, R., Thomas, S., Vasisht, G., Wallace, J. K., Ward-Duong, K., Wiktorowicz, S. J., Wolff, S. G., and Zuckerman, B., "Discovery and spectroscopy of the young jovian planet 51 Eri b with the Gemini Planet Imager," *Science* **350**, 64–67 (Oct. 2015).

[17] Chilcote, J., Pueyo, L., De Rosa, R. J., Vargas, J., Macintosh, B., Bailey, V. P., Barman, T., Bauman, B., Bruzzone, S., Bulger, J., Burrows, A. S., Cardwell, A., Chen, C. H., Cotten, T., Dillon, D., Doyon, R., Draper, Z. H., Duchêne, G., Dunn, J., Erikson, D., Fitzgerald, M. P., Follette, K. B., Gavel, D., Goodsell, S. J., Graham, J. R., Greenbaum, A. Z., Hartung, M., Hibon, P., Hung, L.-W., Ingraham, P., Kalas, P., Konopacky, Q., Larkin, J. E., Maire, J., Marchis, F., Marley, M. S., Marois, C., Metchev, S., Millar-Blanchaer, M. A., Morzinski, K. M., Nielsen, E. L., Norton, A., Oppenheimer, R., Palmer, D.,

Patience, J., Perrin, M., Poyneer, L., Rajan, A., Rameau, J., Rantakyrö, F. T., Sadakuni, N., Saddlemyer, L., Savransky, D., Schneider, A. C., Serio, A., Sivaramakrishnan, A., Song, I., Soummer, R., Thomas, S., Wallace, J. K., Wang, J. J., Ward-Duong, K., Wiktorowicz, S., and Wolff, S., "1-2.4 μm Near-IR Spectrum of the Giant Planet β Pictoris b Obtained with the Gemini Planet Imager," *Astronomical Journal* **153**, 182 (Apr. 2017).

[18] Snellen, I. A. G., Brandl, B. R., de Kok, R. J., Brogi, M., Birkby, J., and Schwarz, H., "Fast spin of the young extrasolar planet β Pictoris b," *Nature* **509**, 63–65 (May 2014).

[19] Wang, J., Mawet, D., Ruane, G., Hu, R., and Benneke, B., "Observing Exoplanets with High Dispersion Coronagraphy. I. The Scientific Potential of Current and Next-generation Large Ground and Space Telescopes," *Astronomical Journal* **153**, 183 (Apr. 2017).

[20] Snellen, I., de Kok, R., Birkby, J. L., Brandl, B., Brogi, M., Keller, C., Kenworthy, M., Schwarz, H., and Stuik, R., "Combining high-dispersion spectroscopy with high contrast imaging: Probing rocky planets around our nearest neighbors," *A&A* **576**, A59 (Apr. 2015).

[21] Lovis, C., Snellen, I., Mouillet, D., Pepe, F., Wildi, F., Astudillo-Defru, N., Beuzit, J.-L., Bonfils, X., Cheetham, A., Conod, U., Delfosse, X., Ehrenreich, D., Figueira, P., Forveille, T., Martins, J. H. C., Quanz, S. P., Santos, N. C., Schmid, H.-M., Ségransan, D., and Udry, S., "Atmospheric characterization of Proxima b by coupling the SPHERE high-contrast imager to the ESPRESSO spectrograph," *A&A* **599**, A16 (Mar. 2017).

[22] Haffert, S. Y., Wilby, M. J., Keller, C. U., and Snellen, I. A. G., "The Leiden EXoplanet Instrument (LEXI): a high-contrast high-dispersion spectrograph," in [*Ground-based and Airborne Instrumentation for Astronomy VI*], *Society of Photo-Optical Instrumentation Engineers (SPIE) Conference Series* **9908**, 990867 (Aug. 2016).

[23] C., S. C., Rus, B., R., B. M., Eric, C., P., C. B., Steve, E., Tyler, G., Sergi, H., John, K., and Douglas, L. P., "The ExoEarth Yield Landscape for Future Direct Imaging Space Telescopes," *arXiv e-prints* , arXiv:1904.11988 (Apr 2019).

[24] Kasdin, N. J., Vanderbei, R. J., Spergel, D. N., and Littman, M. G., "Extrasolar Planet Finding via Optimal Apodized-Pupil and Shaped-Pupil Coronagraphs," *ApJ* **582**, 1147–1161 (Jan. 2003).

[25] Carlotti, A., Kasdin, N. J., Vanderbei, R. J., and Delorme, J.-R., "Optimized shaped pupil masks for pupil with obscuration," in [*Proceedings of the SPIE*], *Proceedings of the SPIE* **8442**, 54 (Sept. 2012).

[26] N'Diaye, M., Pueyo, L., and Soummer, R., "Apodized Pupil Lyot Coronagraphs for Arbitrary Apertures. IV. Reduced Inner Working Angle and Increased Robustness to Low-order Aberrations," *The Astrophysical Journal* **799**, 225 (Feb. 2015).

[27] Give'On, A., Belikov, R., Shaklan, S., and Kasdin, J., "Closed loop, DM diversity-based, wavefront correction algorithm for high contrast imaging systems," *Optics Express* **15**(19), 12338–12343 (2007).

[28] Pueyo, L., Kay, J., Kasdin, N. J., Groff, T., McElwain, M., Give'on, A., and Belikov, R., "Optimal dark hole generation via two deformable mirrors with stroke minimization," *Applied Optics* **48**, 6296 (Nov. 2009).

[29] Belikov, R., Give'on, A., Kern, B., Cady, E., Carr, M., Shaklan, S., Balasubramanian, K., White, V., Echternach, P., Dickie, M., Trauger, J., Kuhnert, A., and Kasdin, N. J., "Demonstration of high contrast in 10% broadband light with the shaped pupil coronagraph," in [*Proceedings of the SPIE*], *Proceedings of the SPIE* **6693**, 66930Y (Sept. 2007).

[30] Cady, E., Prada, C. M., An, X., Balasubramanian, K., Diaz, R., Kasdin, N. J., Kern, B., Kuhnert, A., Nemati, B., Poberezhskiy, I., Eldorado Riggs, A. J., Zimmer, R., and Zimmerman, N., "Demonstration of high contrast with an obscured aperture with the WFIRST-AFTA shaped pupil coronagraph," *Journal of Astronomical Telescopes, Instruments, and Systems* **2**, 011004 (Jan. 2016).

[31] Shi, F., Cady, E., Seo, B.-J., An, X., Balasubramanian, K., Kern, B., Lam, R., Marx, D., Moody, D., and Mejia Prada, C., "Dynamic testbed demonstration of WFIRST coronagraph low order wavefront sensing and control (LOWFS/C)," in [*Procs SPIE*], *Society of Photo-Optical Instrumentation Engineers (SPIE) Conference Series* **10400**, 104000D (Sep 2017).

[32] Balasubramanian, K., White, V., Yee, K., Echternach, P., Muller, R., Dickie, M., Cady, E., Prada, C. M., Ryan, D., Poberezhskiy, I., Kern, B., Zhou, H., Krist, J., Nemati, B., Eldorado Riggs, A. J., Zimmerman, N. T., and Kasdin, N. J., "WFIRST-AFTA coronagraph shaped pupil masks: design, fabrication, and characterization," *Journal of Astronomical Telescopes, Instruments, and Systems* **2**, 011005 (Jan. 2016).

[33] Soummer, R., Brady, G. R., Brooks, K., Comeau, T., Choquet, É., Dillon, T., Egron, S., Gontrum, R., Hagopian, J., Laginja, I., Leboulleux, L., Perrin, M. D., Petrone, P., Pueyo, L., Mazoyer, J., N'Diaye, M., Riggs, A. J. E., Shiri, R., Sivaramakrishnan, A., St. Laurent, K., Valenzuela, A.-M., and Zimmerman, N. T., "High-contrast imager for complex aperture telescopes (HiCAT): 5. first results with segmented-aperture coronagraph and wavefront control," in [*Society of Photo-Optical Instrumentation Engineers (SPIE) Conference Series*], *Society of Photo-Optical Instrumentation Engineers (SPIE) Conference Series* **10698**, 106981O (Aug 2018).

[34] Mawet, D., Serabyn, E., Liewer, K., Hanot, C., McEldowney, S., Shemo, D., and O'Brien, N., "Optical Vectorial Vortex Coronagraphs using Liquid Crystal Polymers: theory, manufacturing and laboratory demonstration," *Optics Express* **17**, 1902–1918 (Feb. 2009).

[35] Mawet, D., Pueyo, L., Carlotti, A., Mennesson, B., Serabyn, E., and Wallace, J. K., "Ring-apodized Vortex Coronagraphs for Obscured Telescopes. I. Transmissive Ring Apodizers," *The Astrophysical Journal Supplement Series* **209**, 7 (Nov. 2013).

[36] Fogarty, K., Pueyo, L., Mazoyer, J., and N'Diaye, M., "Polynomial Apodizers for Centrally Obscured Vortex Coronagraphs," *ApJ* (Mar. 2017).

[37] Pueyo, L. and Norman, C., "High-contrast Imaging with an Arbitrary Aperture: Active Compensation of Aperture Discontinuities," *The Astrophysical Journal* **769**, 102 (June 2013).

[38] Ruane, G., Jewell, J., Mawet, D., Pueyo, L., and Shaklan, S., "Apodized vortex coronagraph designs for segmented aperture telescopes," in [*Proceedings of the SPIE*], *Proceedings of the SPIE* **9912**, 99122L–99122L–13 (2016).

[39] Ruane, G., Mawet, D., Jewell, J., and Shaklan, S., "Performance and sensitivity of vortex coronagraphs on segmented space telescopes," *ArXiv e-prints* (Aug. 2017).

[40] Mazoyer, J., Pueyo, L., N'Diaye, M., Fogarty, K., Zimmerman, N., Soummer, R., Shaklan, and Norman, C., "Active correction of aperture discontinuities - optimized stroke minimization I: a new adaptive interaction matrix algorithm," *submitted to AJ* (2017).

[41] Mazoyer, J., Pueyo, L., N'Diaye, M., Fogarty, K., Zimmerman, N., Soummer, R., Shaklan, and Norman, C., "Active correction of aperture discontinuities - optimized stroke minimization I: a new adaptive control matrix algorithm," *submitted to AJ* (2017).

[42] Ruane, G., Riggs, A., Coker, C. T., Shaklan, S. B., Sidick, E., Mawet, D., Jewell, J., Balasubramanian, K., and Stark, C. C., "Fast linearized coronagraph optimizer (FALCO) IV: coronagraph design survey for obstructed and segmented apertures," in [*Society of Photo-Optical Instrumentation Engineers (SPIE) Conference Series*], *Society of Photo-Optical Instrumentation Engineers (SPIE) Conference Series* **10698**, 106984U (Aug 2018).

[43] Fogarty, K., Pueyo, L., Mazoyer, J., and N'Diaye, M., "Tip/tilt optimizations for polynomial apodized vortex coronagraphs on obscured telescope pupils," in [*Society of Photo-Optical Instrumentation Engineers (SPIE) Conference Series*], *Society of Photo-Optical Instrumentation Engineers (SPIE) Conference Series* **10400**, 104000T (Sept. 2017).

[44] Mawet, D., Serabyn, E., Liewer, K., Burruss, R., Hickey, J., and Shemo, D., "The Vector Vortex Coronagraph: Laboratory Results and First Light at Palomar Observatory," *The Astrophysical Journal* **709**, 53–57 (Jan. 2010).

[45] Mawet, D., Serabyn, E., Moody, D., Kern, B., Niessner, A., Kuhnert, A., Shemo, D., Chipman, R., McClain, S., and Trauger, J., "Recent results of the second generation of vector vortex coronagraphs on the high-contrast imaging testbed at JPL," in [*Proceedings of the SPIE*], *Proceedings of the SPIE* **8151**, 81511D (Oct. 2011).

[46] Serabyn, E., Prada, C. M., Chen, P., and Mawet, D., "Vector vortex coronagraphy for exoplanet detection with spatially variant diffractive waveplates," *Journal of the Optical Society of America B Optical Physics* **36**, D13 (May 2019).

[47] Guyon, O., Pluzhnik, E. A., Galicher, R., Martinache, F., Ridgway, S. T., and Woodruff, R. A., "Exoplanet Imaging with a Phase-induced Amplitude Apodization Coronagraph. I. Principle," *The Astrophysical Journal* **622**, 744–758 (Mar. 2005).

[48] Guyon, O., Hinz, P. M., Cady, E., Belikov, R., and Martinache, F., "High Performance Lyot and PIAA Coronagraphy for Arbitrarily Shaped Telescope Apertures," *Astrophysical Journal* **780**, 171 (Jan 2014).

[49] Belikov, R., Bryson, S., Sirbu, D., Guyon, O., Bendek, E., and Kern, B., "Design and performance analysis of a PIAACMC coronagraph on a segmented aperture," in [*Society of Photo-Optical Instrumentation Engineers (SPIE) Conference Series*], *Society of Photo-Optical Instrumentation Engineers (SPIE) Conference Series* **10698**, 106981H (Aug 2018).

[50] Pluzhnik, E. A., Guyon, O., Ridgway, S. T., Martinache, F., Woodruff, R. A., Blain, C., and Galicher, R., "Exoplanet Imaging with a Phase-induced Amplitude Apodization Coronagraph III. Hybrid Approach: Optical Design and Diffraction Analysis," *arXiv:astro-ph/0512421* (Dec. 2005). arXiv: astro-ph/0512421.

[51] Kern, B., Guyon, O., Belikov, R., Wilson, D., Muller, R., Sidick, E., Balasubramanian, B., Krist, J., Poberezhskiy, I., and Tang, H., "Phase-induced amplitude apodization complex mask coronagraph mask fabrication, characterization, and modeling for WFIRST-AFTA," *Journal of Astronomical Telescopes, Instruments, and Systems* **2**, 011014 (Jan 2016).

[52] Kuchner, M. J. and Traub, W. A., "A Coronagraph with a Band-limited Mask for Finding Terrestrial Planets," *The Astrophysical Journal* **570**, 900–908 (May 2002).

[53] Trauger, J. T. and Traub, W. A., "A laboratory demonstration of the capability to image an Earth-like extrasolar planet," *Nature* **446**, 771–773 (Apr. 2007).

[54] Trauger, J., Gordon, B., Krist, J., and Moody, D., "Hybrid Lyot coronagraph for WFIRST-AFTA: coronagraph design and performance metrics," in [*Proceedings of the SPIE*], *Proceedings of the SPIE* **9605**, 96050N (Sept. 2015).

[55] Seo, B.-J., Cady, E., Gordon, B., Kern, B., Lam, R., Marx, D., Moody, D., Muller, R., Patterson, K., and Poberezhskiy, I., "Hybrid Lyot coronagraph for WFIRST: high-contrast broadband testbed demonstration," in [*Procs SPIE*], *Society of Photo-Optical Instrumentation Engineers (SPIE) Conference Series* **10400**, 104000F (Sep 2017).

[56] Stark, C. C., Roberge, A., Mandell, A., Clampin, M., Domagal-Goldman, S. D., McElwain, M. W., and Stapelfeldt, K. R., "Lower Limits on Aperture Size for an ExoEarth Detecting Coronagraphic Mission," *ApJ* **808**, 149 (Aug 2015).

[57] Groff, T. D., Kasdin, N. J., Carlotti, A., and Riggs, A. J. E., "Broadband focal plane wavefront control of amplitude and phase aberrations," in [*Space Telescopes and Instrumentation 2012: Optical, Infrared, and Millimeter Wave*], *Society of Photo-Optical Instrumentation Engineers (SPIE) Conference Series* **8442**, 84420C (Sept. 2012).

[58] Morgan, R. E., Douglas, E. S., Allan, G. W., Bierden, P., Chakrabarti, S., Cook, T., Egan, M., Furesz, G., Gubner, J. N., Groff, T. D., Haughwout, C. A., Holden, B. G., Mendillo, C. B., Ouellet, M., do Vale Pereira, P., Stein, A. J., Thibault, S., Wu, X., Xin, Y., and Cahoy, K. L., "Mems deformable mirrors for space-based high-contrast imaging," *Micromachines* **10**(6) (2019).

[59] Madec, P. Y., "Overview of deformable mirror technologies for adaptive optics and astronomy," in [*Procs SPIE*], *Society of Photo-Optical Instrumentation Engineers (SPIE) Conference Series* **8447**, 844705 (Jul 2012).

[60] Wirth, A., Cavaco, J., Bruno, T., and Ezzo, K. M., "Deformable mirror technologies at aoa xinetics," (2013).

[61] Allan, G., Douglas, E. S., Barnes, D., Egan, M., Furesz, G., Grunwald, W., Gubner, J., Haughwout, C., Holden, B. G., and do Vale Pereira, P., "The deformable mirror demonstration mission (DeMi) CubeSat: optomechanical design validation and laboratory calibration," in [*Society of Photo-Optical Instrumentation Engineers (SPIE) Conference Series*], *Society of Photo-Optical Instrumentation Engineers (SPIE) Conference Series* **10698**, 1069857 (Aug 2018).

[62] Bordé, P. J. and Traub, W. A., "High-Contrast Imaging from Space: Speckle Nulling in a Low-Aberration Regime," *The Astrophysical Journal* **638**, 488 (Feb. 2006).

[63] Give'on, A., Kern, B., Shaklan, S., Moody, D. C., and Pueyo, L., "Broadband wavefront correction algorithm for high-contrast imaging systems," in [*Proceedings of the SPIE*], *Proceedings of the SPIE* **6691**, 66910A (Sept. 2007).

[64] Shaklan, S. B. and Green, J. J., "Reflectivity and optical surface height requirements in a broadband coronagraph. 1.Contrast floor due to controllable spatial frequencies," *Applied Optics* **45**, 5143–5153 (July 2006).

[65] Pueyo, L. and Kasdin, N. J., "Polychromatic Compensation of Propagated Aberrations for High-Contrast Imaging," *The Astrophysical Journal* **666**, 609–625 (Sept. 2007).

[66] Krist, J., Nemati, B., and Mennesson, B., "Numerical modeling of the proposed WFIRST-AFTA coronagraphs and their predicted performances," *Journal of Astronomical Telescopes, Instruments, and Systems* **2**, 011003 (Jan. 2016).

[67] Armano, M., Audley, H., Baird, J., Binetruy, P., Born, M., Bortoluzzi, D., Castelli, E., Cavalleri, A., Cesarini, A., Cruise, A. M., Danzmann, K., de Deus Silva, M., Diepholz, I., Dixon, G., Dolesi, R., Ferraioli, L., Ferroni, V., Fitzsimons, E. D., Freschi, M., Gesa, L., Gibert, F., Giardini, D., Giusteri, R., Grimani, C., Grzymisch, J., Harrison, I., Heinzel, G., Hewitson, M., Hollington, D., Hoyland, D., Hueller, M., Inchauspé, H., Jennrich, O., Jetzer, P., Karnesis, N., Kaune, B., Korsakova, N., Killow, C. J., Lobo, J. A., Lloro, I., Liu, L., López-Zaragoza, J. P., Maarschalkerweerd, R., Mance, D., Meshksar, N., Martín, V., Martin-Polo, L., Martino, J., Martin-Porqueras, F., Mateos, I., McNamara, P. W., Mendes, J., Mendes, L., Nofrarias, M., Paczkowski, S., Perreur-Lloyd, M., Petiteau, A., Pivato, P., Plagnol, E., Ramos-Castro, J., Reiche, J., Robertson, D. I., Rivas, F., Russano, G., Slutsky, J., Sopuerta, C. F., Sumner, T., Texier, D., Thorpe, J. I., Vetrugno, D., Vitale, S., Wanner, G., Ward, H., Wass, P. J., Weber, W. J., Wissel, L., Wittchen, A., and Zweifel, P., "Beyond the required lisa free-fall performance: New lisa pathfinder results down to 20 μHz," *Phys. Rev. Lett.* **120**, 061101 (Feb 2018).

[68] Nemati, B., Stahl, M. T., Stahl, H. P., and Shaklan, S. B., "The effects of space telescope primary mirror segment errors on coronagraph instrument performance," in [*Society of Photo-Optical Instrumentation Engineers (SPIE) Conference Series*], *Society of Photo-Optical Instrumentation Engineers (SPIE) Conference Series* **10398**, 103980G (Sep 2017).

[69] Saif, B., Greenfield, P., North-Morris, M., Bluth, M., Feinberg, L., Wyant, J. C., and Keski-Kuha, R., "Sub-picometer dynamic measurements of a diffuse surface," *Applied Optics* **58**, 3156 (Apr 2019).

[70] Guyon, O., "Limits of Adaptive Optics for High-Contrast Imaging," *The Astrophysical Journal* **629**, 592–614 (Aug. 2005).

[71] Fusco, T., Petit, C., Rousset, G., Sauvage, J.-F., Dohlen, K., Mouillet, D., Charton, J., Baudoz, P., Kasper, M., Fedrigo, E., Rabou, P., Feautrier, P., Downing, M., Gigan, P., Conan, J.-M., Beuzit, J.-L., Hubin, N., Wildi, F., and Puget, P., "Design of the extreme AO system for SPHERE, the planet finder instrument of the VLT," in [*Proceedings of the SPIE*], *Proceedings of the SPIE* **6272**, 17 (July 2006).

[72] Poyneer, L. A., De Rosa, R. J., Macintosh, B., Palmer, D. W., Perrin, M. D., Sadakuni, N., Savransky, D., Bauman, B., Cardwell, A., and Chilcote, J. K., "On-sky performance during verification and commissioning of the Gemini Planet Imager's adaptive optics system," in [*Adaptive Optics Systems IV*], *Society of Photo-Optical Instrumentation Engineers (SPIE) Conference Series* **9148**, 91480K (Jul 2014).

[73] Fusco, T., Sauvage, J. F., Mouillet, D., Costille, A., Petit, C., Beuzit, J. L., Dohlen, K., Milli, J., Girard, J., and Kasper, M., "SAXO, the SPHERE extreme AO system: on-sky final performance and future improvements," in [*Adaptive Optics Systems V*], *Society of Photo-Optical Instrumentation Engineers (SPIE) Conference Series* **9909**, 99090U (Jul 2016).

[74] Lozi, J., Guyon, O., Jovanovic, N., Takato, N., Singh, G., Norris, B., Okita, H., Bando, T., and Martinache, F., "Characterizing Vibrations at the Subaru Telescope for the Subaru Coronagraphic Extreme Adaptive Optics instrument," *arXiv e-prints* , arXiv:1809.08296 (Sep 2018).

[75] Guyon, O., "Extreme adaptive optics," *Annual Review of Astronomy and Astrophysics* **56**(1), 315–355 (2018).

[76] Mawet, D., Pueyo, L., Lawson, P., Mugnier, L., Traub, W., Boccaletti, A., Trauger, J. T., Gladysz, S., Serabyn, E., Milli, J., Belikov, R., Kasper, M., Baudoz, P., Macintosh, B., Marois, C., Oppenheimer, B., Barrett, H., Beuzit, J.-L., Devaney, N., Girard, J., Guyon, O., Krist, J., Mennesson, B., Mouillet,

D., Murakami, N., Poyneer, L., Savransky, D., Vérinaud, C., and Wallace, J. K., "Review of small-angle coronagraphic techniques in the wake of ground-based second-generation adaptive optics systems," in [*Proceedings of the SPIE*], *Proceedings of the SPIE* **8442**, 04 (Sept. 2012).

[77] Males, J. R., Close, L. M., Miller, K., Schatz, L., Doelman, D., Lumbres, J., Snik, F., Rodack, A., Knight, J., and Van Gorkom, K., "MagAO-X: project status and first laboratory results," in [*Adaptive Optics Systems VI*], *Society of Photo-Optical Instrumentation Engineers (SPIE) Conference Series* **10703**, 1070309 (Jul 2018).

[78] Guyon, O., "Extreme Adaptive Optics," *Annual Review of Astronomy and Astrophysics* **56**, 315–355 (Sep 2018).

[79] Guyon, O. and Males, J., "Adaptive Optics Predictive Control with Empirical Orthogonal Functions (EOFs)," *arXiv e-prints* , arXiv:1707.00570 (Jul 2017).

[80] Poyneer, L. A. and Véran, J.-P., "Optimal modal Fourier-transform wavefront control," *Journal of the Optical Society of America A* **22**, 1515–1526 (Aug. 2005).

[81] Jared R. Males, O. G., "Ground-based adaptive optics coronagraphic performance under closed-loop predictive control," *Journal of Astronomical Telescopes, Instruments, and Systems* **4**(1), 1 – 21 – 21 (2018).

[82] Marois, C., Lafrenière, D., Doyon, R., Macintosh, B., and Nadeau, D., "Angular Differential Imaging: A Powerful High-Contrast Imaging Technique," *The Astrophysical Journal* **641**, 556 (Apr. 2006).

[83] Lafreniere, D., Marois, C., Doyon, R., Nadeau, D., and Artigau, É., "A new algorithm for point-spread function subtraction in high-contrast imaging: A demonstration with angular differential imaging," *The Astrophysical Journal* **660**(1), 770 (2007).

[84] Soummer, R., Pueyo, L., and Larkin, J., "Detection and Characterization of Exoplanets and Disks Using Projections on Karhunen-Loève Eigenimages," *The Astrophysical Journal Letters* **755**, L28 (Aug. 2012).

[85] Jovanovic, N., Absil, O., Baudoz, P., Beaulieu, M., Bottom, M., Cady, E., Carlomagno, B., Carlotti, A., Doelman, D., and Fogarty, K., "Review of high-contrast imaging systems for current and future ground-based and space-based telescopes: Part II. Common path wavefront sensing/control and coherent differential imaging," in [*Society of Photo-Optical Instrumentation Engineers (SPIE) Conference Series*], *Society of Photo-Optical Instrumentation Engineers (SPIE) Conference Series* **10703**, 107031U (Jul 2018).

[86] Debes, J. H., Ren, B., and Schneider, G., "Pushing the Limits of the Coronagraphic Occulters on HST/STIS," *arXiv e-prints* , arXiv:1905.06838 (May 2019).

[87] Perrin, M. D., Pueyo, L., Van Gorkom, K., Brooks, K., Rajan, A., Girard, J., and Lajoie, C.-P., "Updated optical modeling of jwst coronagraph performance contrast, stability, and strategies," (2018).

[88] N'Diaye, M., Dohlen, K., Fusco, T., and Paul, B., "Calibration of quasi-static aberrations in exoplanet direct-imaging instruments with a Zernike phase-mask sensor," *Astronomy and Astrophysics* **555**, A94 (July 2013).

[89] N'Diaye, M., Vigan, A., Dohlen, K., Sauvage, J. F., Caillat, A., Costille, A., Girard, J. H. V., Beuzit, J. L., Fusco, T., and Blanchard, P., "Calibration of quasi-static aberrations in exoplanet direct-imaging instruments with a Zernike phase-mask sensor. II. Concept validation with ZELDA on VLT/SPHERE," *Astronomy and Astrophysics* **592**, A79 (Aug 2016).

[90] Shi, F., Balasubramanian, K., Bartos, R., Hein, R., Lam, R., Mandic, M., Moore, D., Moore, J., Patterson, K., Poberezhskiy, I., Shields, J., Sidick, E., Tang, H., Truong, T., Wallace, J. K., Wang, X., and Wilson, D. W., "Low order wavefront sensing and control for WFIRST coronagraph," in [*Space Telescopes and Instrumentation 2016: Optical, Infrared, and Millimeter Wave*], *Procs SPIE* **9904**, 990418 (July 2016).

[91] Lightsey, P. A., Knight, J. S., and Golnik, G., "Status of the optical performance for the James Webb Space Telescope," in [*Society of Photo-Optical Instrumentation Engineers (SPIE) Conference Series*], *Society of Photo-Optical Instrumentation Engineers (SPIE) Conference Series* **9143**, 914304 (Aug 2014).

[92] Leboulleux, L., Sauvage, J.-F., Pueyo, L. A., Fusco, T., Soummer, R., Mazoyer, J., Sivaramakrishnan, A., N'Diaye, M., and Fauvarque, O., "Pair-based Analytical model for Segmented Telescopes Imaging from Space for sensitivity analysis," *Journal of Astronomical Telescopes, Instruments, and Systems* **4**, 035002 (Jul 2018).

[93] Leboulleux, L., Pueyo, L., Sauvage, J.-F., Fusco, T., Mazoyer, J., Sivaramakrishnan, A., N'Diaye, M., and Soummer, R., "Sensitivity analysis for high-contrast imaging with segmented space telescopes," in [*Society of Photo-Optical Instrumentation Engineers (SPIE) Conference Series*], *Society of Photo-Optical Instrumentation Engineers (SPIE) Conference Series* **10698**, 106986H (Jul 2018).

[94] Dustin B. Moore, D. C. R., "Picometer differential wavefront metrology by nonlinear zernike wavefront sensing for luvoir," (2018).

[95] Douglas, E. S., Males, J. R., Clark, J., Guyon, O., Lumbres, J., Marlow, W., and Cahoy, K. L., "Laser guide star for large segmented-aperture space telescopes. i. implications for terrestrial exoplanet detection and observatory stability," *The Astronomical Journal* **157**, 36 (jan 2019).

[96] Shi, F., Seo, B.-J., Cady, E., Kern, B., Lam, R., Marx, D., Patterson, K., Mejia Prada, C., Shaw, J., Shelton, C., Shields, J., Tang, H., and Truong, T., "WFIRST low order wavefront sensing and control dynamic testbed performance under the flight like photon flux," in [*Society of Photo-Optical Instrumentation Engineers (SPIE) Conference Series*], *Society of Photo-Optical Instrumentation Engineers (SPIE) Conference Series* **10698**, 106982O (Jul 2018).

[97] Singh, G., Lozi, J., Jovanovic, N., Guyon, O., Baudoz, P., Martinache, F., and Kudo, T., "A Demonstration of a Versatile Low-order Wavefront Sensor Tested on Multiple Coronographs," *PASP* **129**, 095002 (Sep 2017).

[98] Riggs, A. J. E., Kasdin, N. J., and Groff, T. D., "Recursive starlight and bias estimation for high-contrast imaging with an extended Kalman filter," *Journal of Astronomical Telescopes, Instruments, and Systems* **2**, 011017 (Jan. 2016).

[99] Pogorelyuk, L. and Kasdin, N. J., "Dark Hole Maintenance and A Posteriori Intensity Estimation in the Presence of Speckle Drift in a High-contrast Space Coronagraph," *ApJ* **873**, 95 (Mar 2019).

[100] Coyle, L. E., Knight, J. S., and Adkins, M., "Edge sensor concept for segment stabilization," in [*Society of Photo-Optical Instrumentation Engineers (SPIE) Conference Series*], *Society of Photo-Optical Instrumentation Engineers (SPIE) Conference Series* **10698**, 1069869 (Jul 2018).

[101] L. D. Feinberg, e. a., "Ultra-stable segmented telescope sensing and control architecture," *Proc. SPIE 10398* (2017).

[102] Lou, J. Z., Redding, D. C., Nissen, J. A., and Shelton, C., "LUVOIR primary mirror segment alignment control with joint laser metrology and segment edge sensing," in [*Society of Photo-Optical Instrumentation Engineers (SPIE) Conference Series*], *Society of Photo-Optical Instrumentation Engineers (SPIE) Conference Series* **10698**, 1069840 (Jul 2018).

[103] Guyon, O., Sevin, A., Gratadour, D., Bernard, J., Ltaief, H., Sukkari, D., Cetre, S., Skaf, N., Lozi, J., and Martinache, F., "The compute and control for adaptive optics (CACAO) real-time control software package," in [*Procs SPIE*], *Society of Photo-Optical Instrumentation Engineers (SPIE) Conference Series* **10703**, 107031E (Jul 2018).

[104] Gratadour, D., Morris, T., Biasi, R., Deneux, H., Bernard, J., Buey, J.-T., Doucet, N., Ferreira, F., Laine, M., and Perret, D., "Prototyping AO RTC using emerging high performance computing technologies with the Green Flash project," in [*Procs SPIE*], *Society of Photo-Optical Instrumentation Engineers (SPIE) Conference Series* **10703**, 1070318 (Jul 2018).

[105] Groff, T. D. and Jeremy Kasdin, N., "Kalman filtering techniques for focal plane electric field estimation," *Journal of the Optical Society of America A* **30**, 128 (Jan. 2013).

[106] Riggs, A. J. E., Kasdin, N. J., and Groff, T. D., "Wavefront correction with Kalman filtering for the WFIRST-AFTA coronagraph instrument," in [*Proceedings of the SPIE*], *Proceedings of the SPIE* **9605**, 960507 (Sept. 2015).

[107] Jackson, K., Wallace, J. K., and Pellegrino, S., "Co-phasing primary mirror segments of an optical space telescope using a long stroke Zernike WFS," in [*Space Telescopes and Instrumentation 2016: Optical, Infrared, and Millimeter Wave*], *Procs SPIE* **9904**, 99046D (July 2016).